Fulde-Ferrell-Larkin-Ovchinnikov states in one-dimensional spin-polarized ultracold atomic Fermi gases

Xia-Ji Liu,[1,2] Hui Hu,[1,2] and Peter D. Drummond[1]

[1]*ARC Centre of Excellence for Quantum-Atom Optics, School of Physical Sciences, University of Queensland, Brisbane, Queensland 4072, Australia*
[2]*Department of Physics, Renmin University of China, Beijing 100872, China*

We present a systematic study of quantum phases in a one-dimensional spin-polarized Fermi gas. Three comparative theoretical methods are used to explore the phase diagram at zero temperature: the mean-field theory with either an order parameter in a single-plane-wave form or a self-consistently determined order parameter using the Bogoliubov–de Gennes equations, as well as the exact Bethe ansatz method. We find that a spatially inhomogeneous Fulde-Ferrell-Larkin-Ovchinnikov phase, which lies between the fully paired Bardeen-Cooper-Schrieffer (BCS) state and the fully polarized normal state, dominates most of the phase diagram of a uniform gas. The phase transition from the BCS state to the Fulde-Ferrell-Larkin-Ovchinnikov phase is of second order, and therefore there are no phase separation states in one-dimensional homogeneous polarized gases. This is in sharp contrast to the three-dimensional situation, where a phase separation regime is predicted to occupy a very large space in the phase diagram. We conjecture that the prediction of the dominance of the phase separation phases in three dimension could be an artifact of the non-self-consistent mean-field approximation, which is heavily used in the study of three-dimensional polarized Fermi gases. We consider also the effect of a harmonic trapping potential on the phase diagram, and find that in this case the trap generally leads to phase separation, in accord with the experimental observations for a trapped gas in three dimensions. We finally investigate the local fermionic density of states of the Fulde-Ferrell-Larkin-Ovchinnikov ansatz. A two-energy-gap structure appears, which could be used as an experimental probe of the Fulde-Ferrell-Larkin-Ovchinnikov states.

I. INTRODUCTION

Since the successful demonstration of a magnetic Feshbach resonance [1] and the creation of optical lattices [2], ultracold atomic Fermi gases have become a topic of great current interest [3]. Thanks to these key tools, the interatomic interactions and even the dimensionality of ultracold atomic Fermi gases can be easily tuned, which makes them ideal candidates to simulate quantum many-particle systems. Therefore, an intriguing opportunity is opened for studying some long-standing problems, such as the crossover from Bardeen-Cooper-Schrieffer (BCS) superfluidity to Bose-Einstein condensate (BEC) [4–9], and models of high-temperature superconductivity. These remarkable prospects have attracted attention from many researchers, ranging from condensed matter physics to atomic molecular and optical physics, and even particle and astrophysics. Experimentally, superfluidity of an ultracold Fermi gas at the strongly interacting BCS-BEC crossover has been strikingly demonstrated [10–21]. This is a landmark achievement in the history of physics.

Recent experiments have now generated ultracold atomic Fermi gases with finite spin polarization [22–27]. That is, the two spin components have unequal populations. However, the physical understanding of the ground state of a polarized atomic gas remains an open question. The standard BCS model—though not quantitatively accurate for strong interactions—is still qualitatively correct when there is no spin polarization. This simply involves Cooper pairing between spin-up and spin-down atoms with opposite momenta

at the same Fermi surface. A polarized Fermi gas cannot be explained within standard BCS theory because the Fermi surfaces of the two spin components are mismatched. Nonstandard forms of pairing must exist to support superfluidity in this polarized environment.

The study of polarized Fermi gases can be traced back to the middle of the 20th century, soon after the seminal BCS theory paper. Similar theoretical proposals were independently given by Fulde and Ferrell [28], and Larkin and Ovchinnikov [29] (FFLO). These authors suggested that Cooper pairs may acquire a finite center-of-mass momentum [30]. In such an ansatz, the two mismatched Fermi surfaces can overlap, thereby supporting a spatially inhomogeneous superfluidity. The search for the existence of the predicted FFLO state has lasted for more than four decades. Only very recently has there been indirect experimental evidence for observing such states in the heavy fermion superconductor $CeCoIn_5$ [31]. Due to the shrinkage of the available phase space for pairing, the FFLO state is now thought to be very fragile in three dimensions. Alternative pairing scenarios include the following: Sarma superfluidity [32–34], a deformed Fermi surface [35–37], and breached pairing [38]. However, at zero temperature these phases may suffer from an instability towards phase separation. As a result, a phase separation regime consisting of a conventional BCS superfluid and a normal fluid may be favored in three dimensions [39].

The above theoretical issues were not completely resolved in current measurements on polarized ^6Li gases near a broad Feshbach resonance, carried out at MIT [22–25] and Rice

university [26,27]. Though a clear quantum phase transition from a superfluid to normal state was observed [22], the nature and the order of the transition could not be determined due to the finite experimental resolution. The presence of a harmonic trap in these experiments caused additional difficulties in interpreting the experimental results. A number of theoretical papers have sought to explain these experiments on polarized atomic Fermi gases [40–84]. From these analyses, the issues that require timely clarification may be summarized as follows:

(A) *Structure and detection of FFLO states*. Despite a long history, the precise structure of the FFLO states remains elusive [30]. Current investigations of FFLO states rely mostly on the use of a single-plane-wave form for the pairing order parameter $\Delta(\mathbf{x})$, where $\Delta(\mathbf{x}) = \Delta_0 \exp[i\mathbf{q} \cdot x]$, as initially proposed by Fulde and Ferrell [28] (FF). Here $\mathbf{q}$ is the center-of-mass momentum of the Cooper pairs, and the ansatz implies that the magnitude of the order parameter and density is constant in space [44,48,65]. The resulting window for the FFLO state in parameter space turns out to be very narrow [44]. Can we expect a larger parameter range after an optimization of the FFLO proposal? Indeed, by improving the form of the order parameter to the Larkin and Ovchinnikov (LO) type, $\Delta(\mathbf{x}) \propto \cos[\mathbf{q} \cdot x]$, Yoshida and Yip have found recently that the FFLO state became more stable [54]. On the other hand, so far there is no conclusive evidence for the experimental observations of FFLO states [30].

(B) *Intrinsic reason for phase separation*. The narrow window of the FFLO state may require phase separation to fill the gap between BCS and FFLO phases in the phase diagram [39]. Experimentally, a shell structure in the density profile of polarized Fermi gases was observed [23,26], suggesting an interior core of a BCS superfluid state with an outer shell of the normal component. Phase separation in trapped systems, however, cannot be used as a definitive support of the existence of phase separation in a homogeneous gas, since the trap favors separation.

(C) *Quantitative approach for polarized Fermi gases at the BCS-BEC crossover*. A more serious problem is the validity of the mean-field approach. The experiments were done in the strongly interacting BCS-BEC crossover regime, where for the quantitative purpose strong pair fluctuations must be taken into account [5–7,9]. Because of the lack of reliable knowledge of the superfluid phase, these pair fluctuations are usually only considered above the superfluid transition temperature [49,55]. For the same reason, numerical quantum Monte Carlo simulations have been restricted to the normal state [56,64] and hence cannot provide useful information for the superfluid state.

To gain a qualitative insight into these crucial points, in a recent paper [85], we have considered a polarized Fermi gas in one dimension (1D) at zero temperature. In this case the model in free space is exactly soluble via a Bethe ansatz solution [86–92]. We have established the 1D phase diagram of the polarized gas, both in the uniform situation and in the experimentally important trapped environment. Complemented by a mean-field Bogoliubov–de Gennes (BdG) calculation, we have shown that a phase similar to the FFLO-type polarized superfluid is the most widespread in the phase diagram. Using a local density approximation to account for

the harmonic trapping potential, we have found that the trap generally leads to phase separation, with at least one FFLO-type phase present at the trap center.

In this paper, we discuss these results in greater detail, and compare them to other approximations. We particularly focus on the self-consistent BdG method, which we previously treated briefly [85]. To address the issue of the different possible FFLO structures, we present a simplified mean-field calculation with a single-plane-wave assumption for the order parameter, and compare it with the self-consistent BdG results. These systematic investigations give rise to a comprehensive quantitative understanding of the 1D polarized Fermi gas. We note that a qualitative picture was also obtained in earlier works, which were based on a nonperturbative bosonization analysis [93] or a mean-field approximation with an additional assumption on the single-particle energy spectrum [94,95]. However, the resulting phase diagram was not conclusive, and the nature of the transition from BCS to FFLO states was under debate [93].

Strictly speaking, any mean-field approach is only valid in the weak coupling limit. As the interaction strength increases, the pair fluctuations become increasingly important, and therefore must be taken into account. This is particularly noticeable in 1D, where true long-range order is completely destroyed by fluctuations in a homogeneous system in the thermodynamic limit [93], according to the well-known Hohenberg-Mermin-Wagner theorem. To avoid this technical difficulty, we therefore understand that the polarized gas under study is confined either in a box with a finite length L or in a harmonic trap (following the experiments), although sometimes we would like to extend the length L to infinity.

The key results of the present work are that the structure of the 1D FFLO state is clarified. The transition from the BCS state to the FFLO state is shown to be smooth, in marked contrast to the prediction of a first-order transition in three dimensions (3D) [44]. Therefore, a 1D phase separation is excluded in the phase diagram of the uniform system. The phase separation in traps found in our previous paper is indeed simply an artifact of the parabolic trap, as we anticipated. It is possible that similar effects are responsible for the phase separation observations in the Rice experiment [26], which uses a high aspect ratio, elongated 3D trap.

It should be emphasized that as well as being an instructive theoretical test bed for the ground state problem for a 3D gas, a 1D polarized Fermi gas in a trap can be realized exactly using two-dimensional optical lattices [96,97]. In these experiments the radial motion of atoms is frozen to zero-point oscillations due to a tight transverse confinement, while the axial motion is weakly confined. Thus, one can realize a low-dimensional quantum many-body system, and experimentally check the many-body predictions directly. This has also been recently carried out for a 1D Bose gas [96,98].

The paper is organized as follows. In the following section, we outline the theoretical model for a 1D spin-polarized Fermi gas. In Sec. III, we characterize the uniform phase diagram by using a simplified mean-field approach with a single-plane-wave-like order parameter, i.e., the so-called FF solution for the FFLO state. This provides us with an approximate picture of the ground state of a 1D polarized gas. An improved self-consistent BdG calculation is then given in

Sec. IV, without any assumption for the order parameter. The underlying structure of the FFLO states at all spin polarizations is then analyzed. The comparison between these two different mean-field approaches shows that the simple FF ansatz fails to capture the correct physics around the BCS-FFLO transition point. It therefore predicts the wrong type of transition. We conclude that in a 3D polarized gas case, the FF ansatz could lead to the same incorrect conclusion. In Sec. V the validity of these 1D mean-field analyses in the weak-coupling or intermediate-coupling regime is checked using exact Bethe ansatz solutions. A quantitative phase diagram of a homogeneous gas is obtained by gathering all the information from these three methods.

In Secs. VI and VII we study the trapped case, using either the self-consistent BdG equations or the exact solution within the local density approximation. We again find a good agreement between these two results for weak and moderate couplings. The phase diagram of the trapped gas is thereby determined. We also calculate the local fermionic density of states of the FFLO states. A two-energy-gap structure is predicted, which is potentially useful for the experimental detection of FFLO states. Finally, Sec. VIII is devoted to the conclusions and some final remarks.

II. MODELS

Consider a polarized Fermi gas with a broad Feshbach resonance in a highly elongated trap formed using a two-dimensional optical lattice [96]. By suitably tuning the lattice depth, the anisotropy aspect ratio $\lambda = \omega_z / \omega_\rho$ of two harmonic frequencies can be extremely small. As long as the Fermi energy associated with the longitudinal motion of the atoms is much smaller than the energy level separation along the transverse direction, i.e., $k_B T \ll \hbar \omega_\rho$ and $N \hbar \omega_z \ll \hbar \omega_\rho$, where N is the total number of atoms, the transverse motion will be essentially frozen out. One ends up with a quasi-one-dimensional system. The effective Hamiltonian of the 1D polarized attractive Fermi gas then may be described by a single channel model [21,99–101],

$$H = \sum_\sigma \int dx \Psi_\sigma^\dagger(x) \left(-\frac{\hbar^2 \nabla^2}{2m} + V_{\text{trap}}(x) - \mu_\sigma \right) \Psi_\sigma(x)$$

$$+ g_{1D} \int dx \Psi_\uparrow^\dagger(x) \Psi_\downarrow^\dagger(x) \Psi_\downarrow(x) \Psi_\uparrow(x), \qquad (2.1)$$

where the pseudospins $\sigma = \uparrow, \downarrow$ denote the two hyperfine states, and $\Psi_\sigma(x)$ is the Fermi field operator that annihilates an atom at position x in the spin σ state. The number of atoms in each spin component is N_σ and the total number of atoms is $N = N_\uparrow + N_\downarrow$. Two different chemical potentials, $\mu_{\uparrow,\downarrow} = \mu \pm \delta\mu$, are introduced to take into account the population imbalance $\delta N = N_\uparrow - N_\downarrow > 0$. The potential $V_{\text{trap}}(x) = m\omega^2 x^2 / 2$ defines a harmonic trap with an oscillation frequency $\omega = \omega_z$ in the axial direction. In such a quasi-one-dimensional geometry, it is shown by Bergeman et al. [102] that the scattering properties of the atoms can be well described using a contact potential $g_{1D}\delta(x)$, where the 1D effective coupling constant $g_{1D} < 0$ may be expressed through the 3D scattering length a_{3D},

$$g_{1D} = \frac{2\hbar^2 a_{3D}}{m a_\rho^2} \frac{1}{(1 - A a_{3D}/a_\rho)}. \qquad (2.2)$$

Here $a_\rho = \sqrt{\hbar/(m\omega_\rho)}$ is the characteristic oscillator length in the transverse axis, and the constant $A = -\zeta(1/2)/\sqrt{2} \simeq 1.0326$ is responsible for the confinement induced Feshbach resonance [102–104], which changes the scattering properties dramatically when the 3D scattering length is comparable to the transverse oscillator length. It is also convenient to express g_{1D} in terms of an effective 1D scattering length, $g_{1D} = -2\hbar^2/(m a_{1D})$, where

$$a_{1D} = -\frac{a_\rho^2}{a_{3D}} \left(1 - A\frac{a_{3D}}{a_\rho} \right) > 0. \qquad (2.3)$$

Note that in the definition of the 1D scattering length, the sign convention is opposite to the 3D case.

In this paper, we will assume a negative 3D scattering length. In other words, the 1D attractive polarized Fermi gas would be obtained experimentally from a 3D polarized gas on the BCS side of the Feshbach resonance magnetic field [105,106].

In the absence of the harmonic trap, we measure the interactions by a dimensionless parameter γ, which is the ratio of the interaction energy density e_{int} to the kinetic energy density e_{kin} [107]. In the weak coupling limit, $e_{\text{int}} \sim g_{1D} n$ and $e_{\text{kin}} \sim \hbar^2 k^2/(2m) \sim \hbar^2 n^2/m$, where n is the total linear density. Therefore, one finds

$$\gamma = -\frac{m g_{1D}}{\hbar^2 n} = \frac{2}{n a_{1D}}. \qquad (2.4)$$

Thus, $\gamma \ll 1$ corresponds to the weakly interacting limit, while the strong coupling regime is realized when $\gamma \gg 1$.

In the case of a trap, we may characterize the interactions using the dimensionless parameter at the trap center $\gamma_0 = \gamma(x=0)$. For an ideal two-component Fermi gas with equal spin populations, the total linear density is

$$n_{\text{ideal}}(x) = n_0 \left(1 - \frac{x^2}{x_{\text{TF}}^2} \right)^{1/2}, \qquad (2.5)$$

in the Thomas-Fermi (TF) approximation, where

$$n_0 = \frac{2N^{1/2}}{\pi a_{ho}}, \qquad (2.6)$$

$$x_{\text{TF}} = N^{1/2} a_{ho}, \qquad (2.7)$$

are, respectively, the center linear density and the TF radius. Here $a_{ho} = \sqrt{\hbar/(m\omega_z)}$ is the characteristic oscillator length in the axial direction. We thus estimate

$$\gamma_0 = \frac{\pi}{N^{1/2}} \left(\frac{a_{ho}}{a_{1D}} \right). \qquad (2.8)$$

In our previous paper [85], we have defined a dimensionless quantity $\kappa = N a_{1D}^2 / a_{ho}^2$ to describe the interactions. These are related via $\gamma_0 = \pi/(\sqrt{\kappa})$.
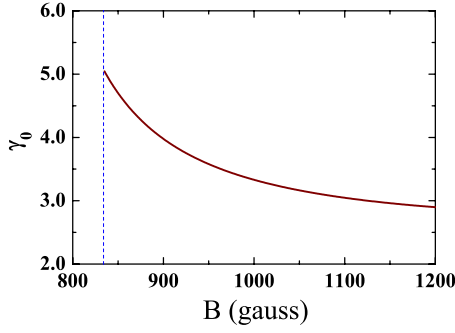
FIG. 1. (Color online) Dimensionless coupling constant at the trap center as a function of the magnetic field. This plot is designed specifically to represent a polarized gas of ^{6}Li atoms in a two-dimensional optical lattice, assuming the same conditions as in the MIT experiment [19]. In detail, we take the total number of atoms as $\sim 10^5$, and therefore in each tube the number of fermions is about $N \sim 100$. The periodicity of the lattice is $d = 532$ nm, yielding a transverse scale $a_\rho \simeq 120$ nm. The axial confinement frequency $\omega \sim 2\pi \times 400$ Hz, giving rise to an axial oscillator length $a_{ho} \simeq 2$ μm. The 3D scattering length is related to the magnetic field via $a_{3d} = -1405a_0[1 + 300/(B-834)][1 + 0.0004(B-834)]$, where the magnetic field B is measured in Gauss and $a_0 = 0.0529$ nm is the Bohr radius. The dashed line in the figure shows the Feshbach resonance field.

Finally, we use a capital $P = (N_\uparrow - N_\downarrow)/N$ to label the total spin polarization, and $p = (n_\uparrow - n_\downarrow)/n$ to denote the local (or uniform) spin polarization.

To make the experimental relevance, we estimate the dimensionless interaction parameters for the on-going experiments on one-dimensional polarized Fermi gases. A gas of ^{6}Li atoms in a three-dimensional optical lattice has been successfully produced by the MIT group [19]. Thus, we consider the case of ^{6}Li gas loaded into a two-dimensional optical lattice with the same parameters. Typically, in each one-dimensional tube the number of ^{6}Li atom is about $N \sim 100$. The transverse oscillator length a_ρ is related to the periodicity of the lattice d via $a_\rho = d/(\pi s^{1/4})$ [108], where s is the ratio of the lattice depth to the recoil energy. Taking $s = 4$, the experimental value of $d = 532$ nm then yields $a_\rho \simeq 120$ nm. An axial confinement of $\omega \sim 2\pi \times 400$ Hz gives rise to an axial oscillator length $a_{ho} = \sqrt{\hbar/(m\omega)} \simeq 2$ μm. Further, the three-dimension scattering length of ^{6}Li gas at the broad resonance is given by [109], $a_{3d} = -1405a_0[1 + 300/(B-834)][1 + 0.0004(B-834)]$, where the magnetic field B is measured in gauss and $a_0 = 0.0529$ nm is the Bohr radius. We then use the relation,

$$\gamma_0 = -\frac{\pi}{N^{1/2}} \frac{a_{ho}a_{3D}}{a_\rho^2} \frac{1}{(1 - Aa_{3D}/a_\rho)}, \quad (2.9)$$

to estimate the dimensionless coupling constant at the trap center.

Figure 1 gives the resulting γ_0 as a function of the magnetic field B. We find that $\gamma_0 \sim O(1)$ above the Feshbach resonance. Throughout this work we shall take a coupling constant of $\gamma = 1.6$. We note that there is already some indi-

rect evidence for superfluidity of a Fermi gas in a three-dimensional optical lattice [19], at the magnetic field considered. On switching to a two-dimensional optical lattice, the temperature in the experiments may still be low enough to generate the various one-dimensional superfluid phases at zero temperature.

Throughout the paper we shall mainly study two different cases, either with a fixed total number of particles and a fixed chemical potential difference, or with given numbers of both spin-up and spin-down particles. The system with two fixed chemical potentials may be considered as well. These three situations require the use of different canonical ensembles in thermodynamics. In the first two cases, we minimize the free energies of the system, $F_{\delta\mu}(T,V,n,\delta\mu)$ and $F_{\delta n}(T,V,n,\delta n)$, respectively, while in the latter case, we minimize instead the thermodynamic potential $\Omega(T,V,\mu,\delta\mu)$.

III. SINGLE-PLANE-WAVE APPROXIMATION IN A HOMOGENEOUS GAS

We first consider a mean-field description with a single-plane-wave FF-type order parameter, to give the simplest qualitative picture of a homogeneous polarized Fermi gas [48]. At this point, we write the Hamiltonian (2.1) in momentum space using a Fourier decomposition of the Fermi field operators. This results in

$$\mathcal{H}_{hom} = \sum_{k\sigma} (\epsilon_k - \mu_\sigma)c_{k\sigma}^\dagger c_{k\sigma}$$
$$+ g_{1D} \sum_{pkk'} c_{p/2+k\uparrow}^\dagger c_{p/2-k\downarrow}^\dagger c_{p/2-k'\downarrow} c_{p/2+k'\uparrow}, \quad (3.1)$$

where $\epsilon_k = \hbar^2 k^2/2m$ is the kinetic energy. The single-plane-wave mean-field approximation amounts to decoupling the interaction term using an order parameter $\Delta = -g_{1D}\sum_k \langle c_{q/2-k\downarrow}c_{q/2+k\uparrow} \rangle$ for the Cooper pairs, where we assume that the pairing occurs between a spin-up atom with a momentum $q/2+k$ and a spin-down atom with a momentum $q/2-k$. As a result, the pairs possess a specific nonzero center-of-mass momentum q, whose value, together with the value of Δ, are to be determined. It is easy to see that after a Fourier transformation, the order parameter in real space acquires a single-plane-wave form, i.e., $\Delta(x) = \Delta \exp(iqx)$. Therefore, within this approximation, we have a mean-field Hamiltonian,

$$\mathcal{H}_{hom}^{MF} = -\frac{\Delta^2}{g_{1D}} - g_{1D}n_\uparrow n_\downarrow + \sum_{k\sigma} (\epsilon_k - \tilde{\mu}_\sigma)c_{k\sigma}^\dagger c_{k\sigma}$$
$$- \Delta \sum_k (c_{q/2-k\downarrow}c_{q/2+k\uparrow} + \text{H.c.}). \quad (3.2)$$

Here, as a consequence of the constant linear density, Hartree terms like $g_{1D}n_{-\sigma}c_{k\sigma}^\dagger c_{k\sigma}$ merely introduce an overall shift for the chemical potentials. We indicate this by introducing the notation $\tilde{\mu}_\sigma = \mu_\sigma - g_{1D}n_{-\sigma}$ for the shifted chemical potentials.

To solve the mean-field Hamiltonian, it is convenient to use a Nambu spinor creation operator $\psi_k^+ = (c_{q/2+k\uparrow}^\dagger, c_{q/2-k\downarrow})$. The Hamiltonian may then be rewritten in a compact bilinear form,

$$\mathcal{H}_{\text{hom}}^{\text{MF}} = \sum_k \psi_k^\dagger [(\epsilon_k^+ - \tilde{\mu})\sigma_z - \Delta\sigma_x + (\epsilon_k^- - \delta\tilde{\mu})]\psi_k - \frac{\Delta^2}{g_{1D}}$$

$$- g_{1D}n_\uparrow n_\downarrow + \sum_k (\epsilon_k - \tilde{\mu} + \delta\tilde{\mu}), \qquad (3.3)$$

where $\epsilon_k^\pm = (\epsilon_{q/2+k} \pm \epsilon_{q/2-k})/2$, and σ_x and σ_z are the Pauli matrices. For convenience, we have defined

$$\tilde{\mu} = \mu - \frac{g_{1D}n}{2}, \qquad (3.4)$$

$$\delta\tilde{\mu} = \delta\mu + \frac{g_{1D}\delta n}{2}. \qquad (3.5)$$

The bilinear Hamiltonian can be easily diagonalized by working out the eigenvalues $E_k^\pm$ and eigenstates $\Phi_k^\pm$ of the two by two matrix $[(\epsilon_k^+ - \tilde{\mu})\sigma_z - \Delta\sigma_x + (\epsilon_k^- - \delta\tilde{\mu})]$. Explicitly, we find that

$$E_k^\pm = \epsilon_k^- - \delta\tilde{\mu} \pm E_k, \qquad (3.6)$$

and

$$\Phi_k^+ = \begin{pmatrix} u_k \\ v_k \end{pmatrix}, \quad \Phi_k^- = \begin{pmatrix} -v_k^* \\ u_k^* \end{pmatrix}, \qquad (3.7)$$

where $E_k = [(\epsilon_k^+ - \tilde{\mu})^2 + \Delta^2]^{1/2}$ and

$$u_k^2 = \frac{1}{2}\left(1 + \frac{\epsilon_k^+ - \tilde{\mu}}{E_k}\right), \qquad (3.8)$$

$$v_k^2 = \frac{1}{2}\left(1 - \frac{\epsilon_k^+ - \tilde{\mu}}{E_k}\right), \qquad (3.9)$$

$$u_k v_k = -\frac{\Delta}{2E_k}. \qquad (3.10)$$

From the eigenstates $\Phi_k^\pm$, it is natural to define Bogoliubov quasiparticle operators, which are given by

$$\begin{pmatrix} \alpha_{k\uparrow} \\ \alpha_{-k\downarrow}^\dagger \end{pmatrix} = \begin{pmatrix} u_k, & v_k^* \\ -v_k, & u_k^* \end{pmatrix}\psi_k. \qquad (3.11)$$

The bilinear mean-field Hamiltonian then becomes

$$\mathcal{H}_{\text{hom}}^{\text{MF}} = -\frac{\Delta^2}{g_{1D}} - g_{1D}n_\uparrow n_\downarrow$$

$$+ \sum_k (\epsilon_k^+ - \tilde{\mu} - E_k) + \sum_k (E_k + \epsilon_k^- - \delta\tilde{\mu})\alpha_{k\uparrow}^+ \alpha_{k\uparrow}$$

$$+ \sum_k (E_k - \epsilon_k^- + \delta\tilde{\mu})\alpha_{k\downarrow}^+ \alpha_{k\downarrow}. \qquad (3.12)$$

The thermodynamic potential is obtained by replacing $\alpha_{k\sigma}^+ \alpha_{k\sigma}$ by its thermal statistical average values, i.e., the Fermi distribution function $f(E_k^\pm) = 1/[\exp(\beta E_k^\pm)+1]$ with $\beta = 1/(k_B T)$ as the inverse temperature. At zero temperature where β goes to infinity, the Fermi distribution function $f(x)$ reduces to a step function $\Theta(-x)$, i.e., $\Theta(x>0)=1$ and $\Theta(x<0)=0$, so the resulting thermodynamic potential has the form

$$\Omega = -\frac{\Delta^2}{g_{1D}} - g_{1D}n_\uparrow n_\downarrow + \sum_k (\epsilon_k^+ - \tilde{\mu} - E_k)$$

$$+ \sum_k (E_k + \epsilon_k^- - \delta\tilde{\mu})\Theta(-E_k^+)$$

$$+ \sum_k (E_k - \epsilon_k^- + \delta\tilde{\mu})\Theta(-E_k^-), \qquad (3.13)$$

The values of the order parameter Δ and of the pairing momentum q are determined by finding the stationary points in the (Δ, q) plane of the thermodynamic potential, i.e., $\partial\Omega/\partial\Delta = 0$ and $\partial\Omega/\partial q = 0$, with given chemical potential difference $\delta\mu$, or the requirement of number conservation, $\delta n = -\partial\Omega/\partial\delta\mu$. This gives us two distinct procedures for defining the mean-field solution, analogous to the grand-canonical (fixed chemical potential difference) and canonical (fixed number difference) ensembles in thermodynamics.

Once these variational variables are obtained, we calculate straightforwardly the total free energies $F_{\delta\mu} = \Omega + \mu n = \tilde{F}_{\delta\mu} + g_{1D}(n^2 + \delta n^2)/4$ or $F_{\delta n} = \Omega + \mu n + \delta\mu\delta n = \tilde{F}_{\delta n} + g_{1D}(n^2 - \delta n^2)/4$ of the gas, depending on whether the chemical potential difference $\delta\mu$ or the number difference $\delta n = n_\uparrow - n_\downarrow$ is fixed, as indicated by the subscript. Note that at zero temperature the value of the free energy $F_{\delta n}$ is equal to the total ground state energy E. We have also defined two free energies $\tilde{F}_{\delta\mu}$ and $\tilde{F}_{\delta n}$ in the absence of the Hartree terms. In the detailed calculations, for a uniform system we take, respectively, the Fermi energy $\epsilon_F = \hbar^2 k_F^2/(2m)$ and the Fermi wave vector $k_F = \pi n/2$ (of a unpolarized ideal gas) as the units of the energy and of the momentum, by letting $\hbar = 1$ and $2m = 1$.

A. Qualitative phase diagrams

Generally, there are several possible stationary solutions in the landscape of the thermodynamic potential. On the weak coupling side we find only three stable competing ground states, corresponding to local minima of the landscape. As shown in Fig. 2 for a coupling constant $\gamma = 1.6$, these are the unpolarized (BCS), partially polarized (FF), and a fully polarized or normal (N) phases. The other two states, denoted as "Sarma" and "saddle point" phases, are unstable with respect to phase separation [48]. Note that in the figure, the order parameter Δ and the center-of-mass momentum q are measured in units of the full gap of an unpolarized gas, $\Delta_0 \simeq 0.346\,58\epsilon_F$. We have fixed the chemical potential at its unpolarized value, $\tilde{\mu} \simeq 1.045\,94\epsilon_F$, and have taken the chemical potential difference to be $\delta\tilde{\mu} = 0.75\Delta_0$.

For an interaction strength $\gamma = 1.6$, the evolution of the ground states with increasing chemical potential difference is given in Fig. 3. Here we search for the ground state by minimizing the free energy $F_{\delta\mu}$. As $\delta\tilde{\mu}$ increases from zero, the free energy of the BCS state is initially lowest, but rises very rapidly. It intersects with that of the FF state at about $\delta\tilde{\mu} = 0.68\Delta_0$. A first-order quantum phase transition then occurs in mean-field theory, since the first-order derivative of free energies at the intersection point is discontinuous. The apparent hysteresis (presence of the FF state before the transition
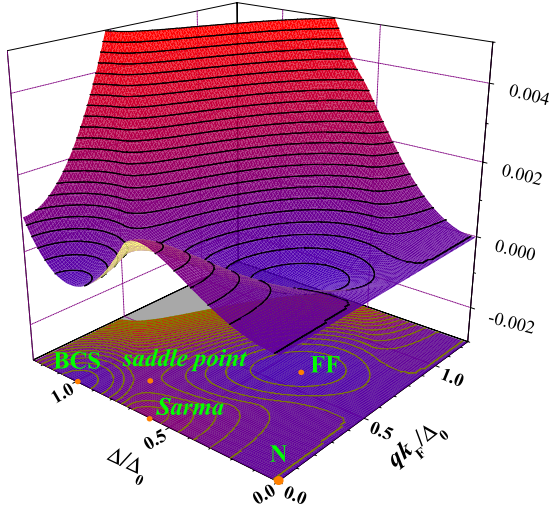
FIG. 2. (Color online) Landscape of the zero-temperature thermodynamic potential of a uniform gas at an interaction strength $\gamma = 1.6$. Here, we take a single-plane-wave approximation for the order parameter, and normalize it using the full gap of an unpolarized Fermi gas, $\Delta_0 = 0.346\,58\epsilon_F$, where ϵ_F is the Fermi energy. The chemical potential is fixed at $\tilde{\mu} = 1.045\,94\epsilon_F$. The competing ground states are (i) a normal Fermi gas with $\Delta = 0$, (ii) a fully paired BCS superfluid with $\Delta = \Delta_0$, $q = 0$, and $\delta n = 0$, (iii) a finite momentum paired FF superfluid with $\Delta < \Delta_0$, $q \neq 0$, and $\delta n \neq 0$, (iv) a breached pairing or Sarma superfluid with $\Delta < \Delta_0$, $q = 0$, and $\delta n \neq 0$, and (v) a saddle point phase intervening between the local BCS and FF minima. We note that the last two phases are unstable with respect to phase separation.

point) is also the mark of a first-order phase transition. After that, the free energy increases slowly towards the normal state value. Precisely at $\delta\tilde{\mu} = 2\epsilon_F$, the gas enters smoothly into a fully polarized normal state, where the spin polarization $p = (n_\uparrow - n_\downarrow)/(n_\uparrow + n_\downarrow)$ is strictly equal to 1. Hence, differing from the 3D situation, a partially polarized normal phase is excluded in 1D. We present, respectively, the value of the order parameter and the spin polarization as a function of the chemical potential difference in Figs. 4(a) and 4(b). The first-
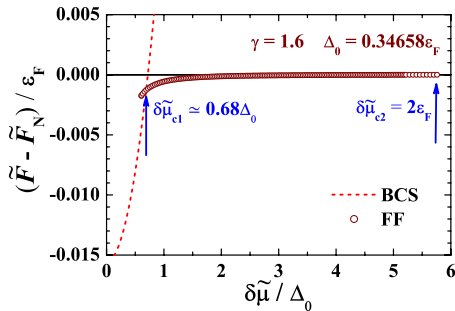

FIG. 3. (Color online) Comparison of the free energies of $\tilde{F}_{\delta\mu}$ available mean-field solutions at a coupling constant $\gamma = 1.6$ and at zero temperature, with the free energy of the normal gas $\tilde{F}_N$ being subtracted. With increasing the chemical potential difference, the gas turns from a BCS superfluid to a FF superfluid at $\delta\tilde{\mu} \simeq 0.68\Delta_0$, and finally becomes a normal gas above $\delta\tilde{\mu} = 2\epsilon_F$.
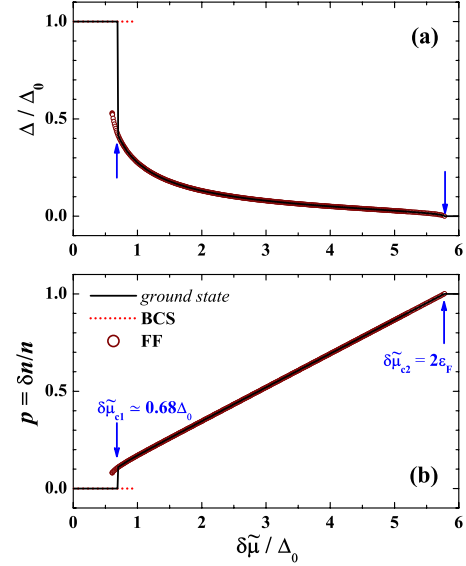

FIG. 4. (Color online) Evolution of the mean-field (FF) order parameter and of the spin polarization, with increasing chemical potential difference. The arrows point to the phase transition positions. The parameters are the same as in Fig. 3.

order transition from BCS to FF states becomes much apparent due to the jump of the order parameter and of the spin polarization. We will show later, however, that this apparent first-order transition is simply an artifact of the single-plane-wave approximation for the order parameter.

By changing the coupling constant, we can determine a phase diagram in the plane of the interaction strength γ and chemical potential difference $\delta\tilde{\mu}$, as shown in Fig. 5(a). The solid and dashed lines separate the FF state from the normal and BCS phases, respectively, and converge to a single curve above $\gamma \simeq 7$. Converting the chemical potential difference to a number difference, we obtain a phase diagram in the γ-p plane in Fig. 5(b). The area under the dashed line has no correspondence in Fig. 5(a) and belongs to the "saddle point" solution, which is unstable towards phase separation. This may be the precursor of a phase separation phase. Overall, all the basic features found here are qualitatively similar to that in 3D [48].

B. Analytic results in limiting cases

We discuss some analytic results that can be obtained in the weakly interacting limit of $\gamma \to 0$. The simplest one is the unpolarized BCS state, for which the chemical potential $\tilde{\mu}$ is essentially the Fermi energy ϵ_F. The stationary condition $\partial\Omega/\partial\Delta = 0$ then leads to a gap equation,

$$\frac{1}{g_{1D}} + \sum_k \frac{1}{2\sqrt{(\epsilon_k - \epsilon_F)^2 + \Delta_0^2}} = 0. \quad (3.14)$$

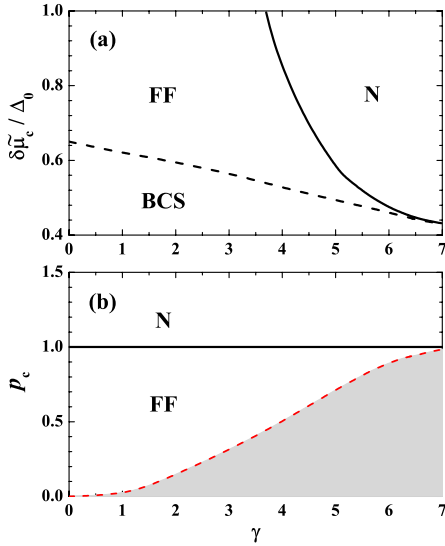The integration can be worked out analytically for small Δ_0. One finds that

FIG. 5. (Color online) (a) Phase diagram in the plane of the interaction strength and the chemical potential difference. Within the single-plane-wave assumption for the order parameter, the transition from a BCS superfluid to a FF state is of first order (dashed line), while from a FF state to the normal state it is continuous (solid line). (b) Interaction strength vs polarization phase diagram. The shadow region is unknown, and presumably is an artifact of the single-plane-wave approximation.

$$\Delta_0 \simeq 8\epsilon_F \exp\left(-\frac{\pi^2}{2\gamma}\right), \tag{3.15}$$

analogous to the standard 3D BCS result $\Delta_0^{3D} \simeq 8\epsilon_F \exp[\pi/(2k_F a)-2]$. For the FF state at a large chemical potential difference, the value of the order parameter is even smaller. To a good approximation, we find that

$$\tilde{\mu} \simeq \epsilon_F + \frac{(\delta\tilde{\mu})^2}{4\epsilon_F}, \tag{3.16}$$

$$qk_F \simeq \delta\tilde{\mu}, \tag{3.17}$$

and hence

$$\Delta = 8\epsilon_F \frac{\sqrt{(2\epsilon_F - \delta\tilde{\mu})(2\epsilon_F + \delta\tilde{\mu})}}{\delta\tilde{\mu}} \exp\left(-\frac{\pi^2}{\gamma}\right). \tag{3.18}$$

From the prefactor, the order parameter Δ vanishes exactly at $\delta\tilde{\mu}=2\epsilon_F$. At the same time $\tilde{\mu}=2\epsilon_F$, indicating that the FF state changes smoothly into a fully polarized normal state.

C. Local fermionic density of states

The Bogoliubov quasiparticle amplitudes (u_k, v_k) and energy E_k appear in the zero temperature spectrum of the single fermionic excitations. We characterize the excitation spectrum using the local fermionic density of states, $\rho_\sigma(\epsilon)$, given by

$$\rho_\uparrow(\epsilon) = \sum_{\mathbf{k}} u_k^2 \delta(\epsilon - E_k^+) + \sum_{\mathbf{k}} v_k^2 \delta(\epsilon - E_k^-), \tag{3.19}$$
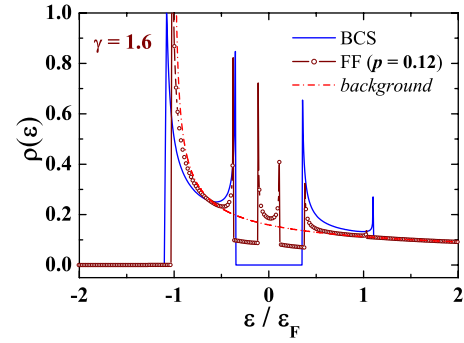

FIG. 6. (Color online) Local fermionic density of states of a uniform polarized Fermi gas, with a single-plane-wave form for the order parameter. Note that there is a prominent two-energy-gap structure in the FF state.

$$\rho_\downarrow(\epsilon) = \sum_{\mathbf{k}} v_k^2 \delta(\epsilon + E_k^+) + \sum_{\mathbf{k}} u_k^2 \delta(\epsilon + E_{\mathbf{k}}^-). \tag{3.20}$$

For an ideal gas with equal populations, the density of states can be calculated analytically,

$$\rho_\uparrow^{bk}(\epsilon) = \rho_\downarrow^{bk}(\epsilon) = \frac{\sqrt{2m}}{2\pi\hbar} \frac{1}{\sqrt{\epsilon + \tilde{\mu}}}, \tag{3.21}$$

which we have regarded as a background density of states. It has a band edge (square root) singularity at $\epsilon=-\tilde{\mu}$.

We plot in Fig. 6 the local density of states for a one-dimensional BCS superfluid, and the FF phase at $p=0.12$, as well as the background density of states. In an FF state, the spin-up and spin-down density of states are exactly the same, but are shifted downwards or upwards, respectively, by an amount $\delta\tilde{\mu}$. For clarity, in the figure we show only one branch, i.e., the spin-up density of states after an upwards shift. Compared to the BCS superfluid, the local density of states of the FF phase exhibits an intriguing two-energy-gap structure. The midgap state around $\epsilon=0$ is a salient feature of the spatially modulated order parameter [94].

IV. SELF-CONSISTENT BdG IN A HOMOGENEOUS GAS

We now turn to a more realistic mean-field calculation without resorting any approximation for the form of the order parameter. We consider the BdG equations of the 1D polarized Fermi gas [51,110], starting from the Heisenberg equation of motion of the Hamiltonian (2.1) for $\Psi_\uparrow(x,t)$ and $\Psi_\downarrow(x,t)$ (without the trap potential),

$$i\hbar\frac{\partial\Psi_\uparrow}{\partial t} = \left(-\frac{\hbar^2\nabla^2}{2m} - \mu_\uparrow\right)\Psi_\uparrow + g_{1D}\Psi_\downarrow^+\Psi_\downarrow\Psi_w, \tag{4.1}$$

$$i\hbar\frac{\partial\Psi_\downarrow}{\partial t} = \left(-\frac{\hbar^2\nabla^2}{2m} - \mu_\downarrow\right)\Psi_\downarrow - g_{1D}\Psi_\uparrow^+\Psi_\downarrow\Psi_\uparrow. \tag{4.2}$$

Within the mean-field approximation, we replace the terms $g_{1D}\Psi_\downarrow^+\Psi_\downarrow\Psi_\uparrow$ and $g_{1D}\Psi_\uparrow^+\Psi_\downarrow\Psi_\uparrow$ by their respective mean-field decoupling

$$g_{1D}\Psi_\downarrow\Psi_\uparrow\Psi_\downarrow^+ = -\Delta(x)\Psi_\downarrow^+ + g_{1D}n_\downarrow(x)\Psi_\uparrow, \qquad (4.3)$$

and

$$g_{1D}\Psi_\downarrow\Psi_\uparrow\Psi_\uparrow^+ = -\Delta(x)\Psi_\uparrow^+ + g_{1D}n_\uparrow(x)\Psi_\downarrow, \qquad (4.4)$$

where we have defined an order parameter $\Delta(x) = -g_{1D}\langle\Psi_\downarrow(x)\Psi_\uparrow(x)\rangle$ and densities $n_\sigma(x) = \langle\Psi_\sigma^+(x)\Psi_\sigma(x)\rangle$. The above decoupling thus yields,

$$i\hbar\frac{\partial\Psi_\uparrow}{\partial t} = (\mathcal{H}_\uparrow^s - \mu_\uparrow)\Psi_\uparrow - \Delta(x)\Psi_\downarrow^+, \qquad (4.5)$$

$$i\hbar\frac{\partial\Psi_\downarrow}{\partial t} = (\mathcal{H}_\downarrow^s - \mu_\downarrow)\Psi_\downarrow + \Delta(x)\Psi_\uparrow^+, \qquad (4.6)$$

where $\mathcal{H}_\sigma^s = -\hbar^2\nabla^2/(2m) + g_{1D}n_{\bar\sigma}(x)$. We solve the equation of motion by inserting the standard Bogoliubov transformation

$$\Psi_\uparrow = \sum_\eta [u_{\eta\uparrow}(x)c_{\eta\uparrow}e^{-iE_{\eta\uparrow}t/\hbar} + v_{\eta\downarrow}^*(x)c_{\eta\downarrow}^\dagger e^{iE_{\eta\downarrow}t/\hbar}],$$

$$\Psi_\downarrow^+ = \sum_\eta [u_{\eta\downarrow}^*(x)c_{\eta\downarrow}^\dagger e^{iE_{\eta\downarrow}t/\hbar} - v_{\eta\uparrow}(x)c_{\eta\uparrow}e^{-iE_{\eta\uparrow}t/\hbar}]. \quad (4.7)$$

This gives rise to the well-known BdG equations for the Bogoliubov quasiparticle [110],

$$\begin{bmatrix} \mathcal{H}_\sigma^s - \mu_\sigma & -\Delta(x) \\ -\Delta^*(x) & -\mathcal{H}_{\bar\sigma}^s + \mu_{\bar\sigma} \end{bmatrix} \begin{bmatrix} u_{\eta\sigma} \\ v_{\eta\sigma} \end{bmatrix} = E_{\eta\sigma} \begin{bmatrix} u_{\eta\sigma} \\ v_{\eta\sigma} \end{bmatrix}, \quad (4.8)$$

where the wave functions $u_{\eta\sigma}(x)$ and $v_{\eta\sigma}(x)$ are normalized by

$$\int dx[|u_{\eta\sigma}(x)|^2 + |v_{\eta\sigma}(x)|^2] = 1, \qquad (4.9)$$

and $E_{\eta\sigma}$ is the corresponding excitation energy.

We note that the unequal chemical potentials of spin states in the BdG equations break the particle-hole symmetry. This leads to different quasiparticle wave functions for the two components. However, one may easily identify a one-to-one correspondence between the solution for the spin-up and spin-down energy levels, i.e.,

$$E_{\eta\sigma} \leftrightarrow -E_{\eta\bar\sigma}, \qquad (4.10)$$

and

$$\begin{bmatrix} u_{\eta\sigma}(x) \\ v_{\eta\sigma}(x) \end{bmatrix} \leftrightarrow \begin{bmatrix} -v_{\eta\bar\sigma}^*(x) \\ +u_{\eta\bar\sigma}^*(x) \end{bmatrix}. \qquad (4.11)$$

Because of this symmetry of the BdG equations, therefore, we may consider the spin-up part only. Letting $u_\eta(x) = u_{\eta\uparrow}(x)$ and $v_\eta(r) = v_{\eta\uparrow}(x)$, we then remove the spin index in the equations,

$$\begin{bmatrix} \mathcal{H}_\uparrow^s - \mu_\uparrow & -\Delta(x) \\ -\Delta^*(x) & -\mathcal{H}_\downarrow^s + \mu_\downarrow \end{bmatrix} \begin{bmatrix} u_\eta(x) \\ v_\eta(x) \end{bmatrix} = E_\eta \begin{bmatrix} u_\eta(x) \\ v_\eta(x) \end{bmatrix}. \quad (4.12)$$

The order parameter $\Delta(x)$ and the linear number densities $n_\sigma(x)$ should be determined self-consistently, according to their definitions, respectively,

$$n_\uparrow(x) = \sum_\eta u_\eta^*(x)u_\eta(x)f(E_\eta), \qquad (4.13)$$

$$n_\downarrow(x) = \sum_\eta v_\eta^*(x)v_\eta(x)f(-E_\eta), \qquad (4.14)$$

$$\Delta(x) = -g_{1D}\sum_\eta u_\eta(x)v_\eta^*(x)f(E_\eta), \qquad (4.15)$$

where the summation runs over all the energy levels, including these with negative energies $E_\eta < 0$.

We note also that the single-plane-wave approximation described in the last section can be recovered by replacing the level index "η" with a wave vector k, and approximating,

$$u_\eta(x) = \bar{u}_k \exp\left[+i\left(\frac{q}{2}+k\right)x\right], \qquad (4.16)$$

$$v_\eta(x) = \bar{v}_k \exp\left[-i\left(\frac{q}{2}-k\right)x\right], \qquad (4.17)$$

$$E_\eta = \bar{E}_k, \qquad (4.18)$$

so that the order parameter reduces to

$$\Delta(x) = -g_{1D}\sum_k \bar{u}_k\bar{v}_k f(\tilde{E}_k)\exp(iqx) = \Delta\exp(iqx), \qquad (4.19)$$

and the BdG equations become

$$\begin{bmatrix} \epsilon_{q/2+k} - \tilde{\mu}_\uparrow & -\Delta \\ -\Delta & -\epsilon_{q/2-k} + \tilde{\mu}_\downarrow \end{bmatrix} \begin{bmatrix} \bar{u}_k \\ \bar{v}_k \end{bmatrix} = \bar{E}_k \begin{bmatrix} \bar{u}_k \\ \bar{v}_k \end{bmatrix}, \quad (4.20)$$

where as before, we have used the notations $\tilde{\mu}_\uparrow = \mu_\uparrow - g_{1D}n_\downarrow$ and $\tilde{\mu}_\downarrow = \mu_\downarrow - g_{1D}n_\uparrow$. Apparently, there are two branch solutions for the quasiparticle energy $E_k^+ = (\epsilon_{q/2+k} - \epsilon_{q/2-k})/2 - \delta\tilde{\mu} + E_k$ and $E_k^- = (\epsilon_{q/2+k} - \epsilon_{q/2-k})/2 - \delta\tilde{\mu} - E_k$, with the corresponding quasiparticle wave functions,

$$\begin{pmatrix} \bar{u}_k \\ \bar{v}_k \end{pmatrix}_{\bar{E}_k = E_k^+} = \begin{pmatrix} u_k \\ v_k \end{pmatrix} = \Phi_k^+ \qquad (4.21)$$

and

$$\begin{pmatrix} \bar{u}_k \\ \bar{v}_k \end{pmatrix}_{\bar{E}_k = E_k^-} = \begin{pmatrix} -v_k^* \\ u_k^* \end{pmatrix} = \Phi_k^-, \qquad (4.22)$$

respectively, exactly the same as in Eqs. (3.6) and (3.7). Accordingly, the linear densities take the form

$$n_\uparrow(x) = \sum_k u_k^2 f(E_k^+) + \sum_k v_k^2 f(E_k^-), \qquad (4.23)$$

$$n_\downarrow(x) = \sum_k v_k^2 f(-E_k^+) + \sum_k u_k^2 f(-E_k^-), \quad (4.24)$$

which turn out to be position independent due to the plane-wave form of the wave functions.

A. Hybrid BdG strategy

We apply the above BdG formalism to a uniform Fermi gas with finite atoms. To this end, we consider a gas of N fermions in a box of length L using periodic boundary conditions, i.e., the underlying wave function $\varphi(x)$ satisfies $\varphi(x=+L/2)=\varphi(x=-L/2)$. The small boundary effect due to the finite size of L could be weakened or removed by enlarging the value of L.

In any practical calculation, because of the computational limitations, the summation over the quasiparticle energy levels in Eqs. (4.13)–(4.15) must be truncated. We therefore following the idea of Reidl *et al.* [111] develop a hybrid approach with the introduction of a high-energy cutoff E_c, below which we solve the discrete BdG equations. Above the cutoff, we use a semiclassical plane-wave approximation for the wave functions, which should work well for sufficiently high-lying states.

The first step toward solving the discrete BdG equations is to assume a real order parameter $\Delta(x)$ and then expand the quasiparticle wave functions $u(x)$ and $v(x)$ using a complete basis of single particle wave functions in the box $\varphi_n(x)$ with energy levels ϵ_n ($n=0,1,2,\ldots$), i.e.,

$$u(x) = \sum_n A_n \varphi_n(x), \quad (4.25)$$

$$v(x) = \sum_n B_n \varphi_n(x). \quad (4.26)$$

For the case of periodic boundary condition, we take

$$\varphi_n(x) = \begin{cases} \sqrt{2/L}\cos[n\pi x/L] & \text{if } n \text{ is even,} \\ \sqrt{2/L}\sin[(n+1)\pi x/L] & \text{if } n \text{ is odd,} \end{cases} \quad (4.27)$$

and

$$\epsilon_n = \begin{cases} \hbar^2\pi^2 n^2/(2mL^2) & \text{if } n \text{ is even,} \\ \hbar^2\pi^2(n+1)^2/(2mL^2) & \text{if } n \text{ is odd,} \end{cases} \quad (4.28)$$

The solution of the BdG equations then becomes a matrix diagonalization problem,

$$\begin{bmatrix} \mathcal{H}_{nn'}^{0\uparrow} + \mathcal{M}_{nn'}^{\uparrow} & -\Delta_{nn'} \\ -\Delta_{nn'} & -\mathcal{H}_{nn'}^{0\downarrow} - \mathcal{M}_{nn'}^{\downarrow} \end{bmatrix} \begin{bmatrix} A_{n'} \\ B_{n'} \end{bmatrix} = E \begin{bmatrix} A_n \\ B_n \end{bmatrix}, \quad (4.29)$$

where the matrix elements are

$$\mathcal{H}_{nn'}^{0\sigma} = (\epsilon_n - \mu_\sigma)\delta_{nn'}, \quad (4.30)$$

$$\mathcal{M}_{nn'}^{\sigma} = g_{1D} \int_{-L/2}^{+L/2} dx\, \varphi_n(x) n_{\bar\sigma}(x) \varphi_{n'}(x), \quad (4.31)$$

$$\Delta_{nn'} = \int_{-L/2}^{+L/2} dx\, \varphi_n(x)\Delta(x)\varphi_{n'}(x). \quad (4.32)$$

The coefficients of the eigenstate must satisfy the condition $\sum_n(A_n^2+B_n^2)=1$ due to the normalization of the quasiparticle wavefunctions, i.e., $\int_{-L/2}^{+L/2}dx[u^2(x)+v^2(x)]=1$.

These discrete spectra (labeled by an index "η") contribute to the linear densities and the order parameter as follows:

$$n_{\uparrow d}(x) = \sum_{|E_\eta|<E_c} u_\eta^*(x)u_\eta(x)f(E_\eta), \quad (4.33)$$

$$n_{\downarrow d}(x) = \sum_{|E_\eta|<E_c} v_\eta^*(x)v_\eta(x)f(-E_\eta), \quad (4.34)$$

$$\Delta_d(x) = -g_{1D}\sum_{|E_\eta|<E_c} u_\eta(x)v_\eta^*(x)f(E_\eta), \quad (4.35)$$

where the subscript "d" refers to the discrete levels.

On the other hand, for the high-lying states we take the semiclassical approximation [111],

$$u_\eta(x) \rightarrow u(k,x)\exp(ikx), \quad (4.36)$$

$$v_\eta(x) \rightarrow v(k,x)\exp(ikx), \quad (4.37)$$

$$E_\eta \rightarrow E(k), \quad (4.38)$$

where we have regarded the wave functions locally at position x as plane waves, whose amplitudes $u(k,x)$ and $v(k,x)$ are normalized according to $u^2(k,x)+v^2(k,x)=1$. Keeping the most important pair correlation terms only, it is straightforward to show that at low temperatures,

$$n_{\uparrow c}(x) = \sum_k \left(\frac{1}{2} - \frac{\epsilon_k - \mu}{2E_k(x)}\right)\Theta[E_k(x) + \delta\mu - E_c], \quad (4.39)$$

$$n_{\downarrow c}(x) = \sum_k \left(\frac{1}{2} - \frac{\epsilon_k - \mu}{2E_k(x)}\right)\Theta[E_k(x) - \delta\mu - E_c], \quad (4.40)$$

$$\Delta_c(x) = -g_{1D}\sum_k \frac{\Delta(x)}{2E_k(x)}\Theta[E_k(x) + \delta\mu - E_c], \quad (4.41)$$

where $E_k(x)=\sqrt{(\epsilon_k-\mu)^2+\Delta^2(x)}$ and the subscript "c" means the continuous contribution from high-energy levels.

The discrete and continuous parts of the order parameter may be combined together to give

$$\Delta(x) = -g_{1D}^{\text{eff}}(x)\sum_{|E_\eta|<E_c} u_\eta(x)v_\eta^*(x)f(E_\eta), \quad (4.42)$$

where we have defined a position-dependent effective 1D coupling constant $g_{1D}^{\text{eff}}(x)$, which satisfies

$$\frac{1}{g_{1D}^{\text{eff}}(x)} = \frac{1}{g_{1D}} + g(x), \quad (4.43)$$

where

$$g(x) = \sum_k \frac{1}{2E_k(x)} \Theta[E_k(x) + \delta\mu - E_c]. \qquad (4.44)$$

The summation over the momentum k may be converted into a continuous integral of the energy. As a result, we obtain

$$n_{\uparrow c}(x) = \frac{(2m)^{1/2}}{4\pi\hbar} \int_{E_c}^{\infty} d\epsilon \left(\frac{\epsilon - \delta\mu}{\sqrt{(\epsilon - \delta\mu)^2 - \Delta^2(x)}} - 1 \right)$$

$$\times \frac{1}{[\mu + \sqrt{(\epsilon - \delta\mu)^2 - \Delta^2(x)}]^{1/2}}, \qquad (4.45)$$

$$n_{\downarrow c}(x) = \frac{(2m)^{1/2}}{4\pi\hbar} \int_{E_c}^{\infty} d\epsilon \left(\frac{\epsilon + \delta\mu}{\sqrt{(\epsilon + \delta\mu)^2 - \Delta^2(x)}} - 1 \right)$$

$$\times \frac{1}{[\mu + \sqrt{(\epsilon + \delta\mu)^2 - \Delta^2(x)}]^{1/2}}, \qquad (4.46)$$

and

$$g(x) = \frac{(2m)^{1/2}}{4\pi\hbar} \int_{E_c}^{\infty} d\epsilon \frac{1}{\sqrt{(\epsilon - \delta\mu)^2 - \Delta^2(x)}}$$

$$\times \frac{1}{[\mu + \sqrt{(\epsilon - \delta\mu)^2 - \Delta^2(x)}]^{1/2}}. \qquad (4.47)$$

We can now summarize the entire procedure used to obtain the BdG solutions. The key step is to solve the eigenvalue problem (4.29). As the calculation of matrix elements involves the order parameter and linear densities that are yet to be determined, a self-consistent iterative procedure is required. For a given number of atoms ($N = N_\uparrow + N_\downarrow$ and $\delta N = N_\uparrow - N_\downarrow$), temperature and interaction coupling g_{1D}, we

(a) start with an initial guess or a previously determined better estimate for $\Delta(x)$,

(b) solve Eqs. (4.43) and (4.47) for the effective coupling constant,

(c) then solve Eq. (4.29) for all the quasiparticle wave functions up to the chosen energy cutoff to find $u_\eta(x)$ and $v_\eta(x)$, and finally determine an improved value for the order parameter from Eq. (4.42).

During the iteration, the density profiles $n_\uparrow(x) = n_{\uparrow d}(x) + n_{\uparrow c}(x)$ and $n_\downarrow(x) = n_{\downarrow d}(x) + n_{\downarrow c}(x)$ are updated. The chemical potentials μ and $\delta\mu$ are also adjusted slightly in each iterative step to enforce the number-conservation condition that $\int_{-L/2}^{+L/2} dx [n_\uparrow(x) + n_\downarrow(x)] = N$ and $\int_{-L/2}^{+L/2} dx [n_\uparrow(x) - n_\downarrow(x)] = \delta N$, until final convergence is reached.

B. The structure of FFLO states

Using the self-consistent BdG formalism we can work out the detailed structure of mean-field or FFLO states. To make the equations dimensionless, as before we take the Fermi wave vector $k_F = \pi n/2 = \pi N/(2L)$ and the Fermi energy $\epsilon_F = \hbar^2 k_F^2/(2m)$ as the units of the momentum and energy, respectively, i.e., by setting $\hbar = 1$ and $2m = 1$, and $k_F = 1$. Therefore, the size of the box $L = \pi N/2$ can be enlarged by increasing the number of total atoms N. In the following calculations, we use $N = 200$, which in most cases we find is
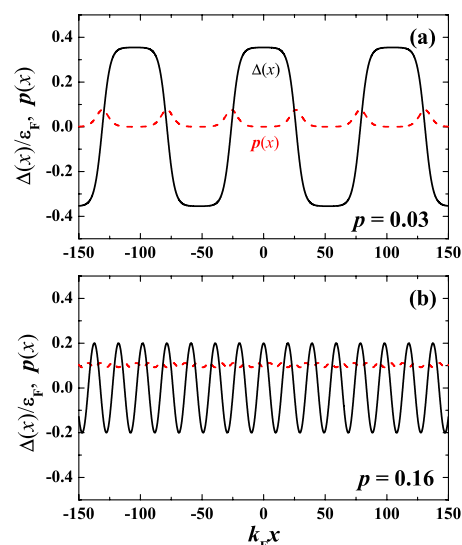

FIG. 7. (Color online) Spatial structures of the inhomogeneous FFLO states at an interaction strength $\gamma = 1.6$ and at two spin polarizations as indicated. The calculations have been done for a uniform gas confined in a box, using the self-consistent BdG equations. The solid line and the dashed line refer to the order parameter and the local spin polarization, respectively.

large enough to effectively minimize the boundary effects. Further, we take a cutoff energy $E_c = 16\epsilon_F$. This cutoff energy is already large because of the high efficiency of our hybrid strategy. Accordingly, we set up a set of single-particle-state basis $\varphi_n(x)$, with the highest energy level larger than the cutoff energy.

The initial guess for the order parameter $\Delta(x)$ could be arbitrary. However, we find that in general there are many locally metastable solutions after the iteration, which can be classified uniquely by their periodicity. This is due to the existence of the periodic boundary condition that requires that the order parameter should be a periodic function of length L/n, where n is an integer. We therefore compare the energy (or free energy) of the solutions with different periodicity, and select the one with the lowest energy as the ground state.

We present in Fig. 7 the spatial distribution of the order parameter $\Delta(x)$ and the local spin polarization

$$p(x) = \frac{n_\uparrow(x) - n_\downarrow(x)}{n_\uparrow(x) + n_\downarrow(x)} \qquad (4.48)$$

for a uniform Fermi gas with total polarization $p = 0.03$ (a) and $p = 0.16$ (b) at a typical coupling constant $\gamma = 1.6$. The most notable feature of the figure is that at a small total polarization [Fig. 7(a)], the order parameter switches between two values: $+\Delta_0$ and $-\Delta_0$, where Δ_0 is the full gap of an unpolarized gas at the same coupling. Many instantons and anti-instantons (or kinks and antikinks) then appear and carry the excess spin-up (majority) atoms since the local polarization $p(x)$ shows pronounced peaks right at the position where the order parameter vanishes. These features are not unlike a phase separation, except that a regular, periodic do-
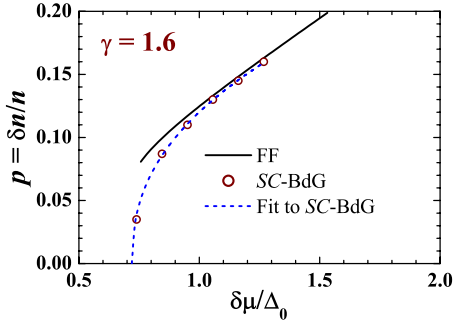
FIG. 8. (Color online) Spin polarization versus the chemical potential difference at an interaction strength $\gamma=1.6$, obtained from the single-plane-wave approximation (solid line) and the self-consistent BdG calculations (open circles). While the spin polarization in the FF state shows a jump as a function of the chemical potential difference, the more accurate self-consistent BdG prediction suggests that the spin polarization emerges from zero continuously with increasing the chemical potential difference. The dashed line is a power-law fit to the self-consistent BdG results.

main structure is obtained. Thus, in the limit of small polarization, the order parameter may be viewed as an instanton gas, with the number of instantons roughly proportional to the spin polarization. Within this picture, we anticipate that an FFLO state emerges as soon as the polarization becomes nonzero. In contrast, for a large total polarization [Fig. 7(b)], the order parameter is well approximated by a cosine function, as expected earlier by Larkin and Ovchinnikov. It is a superposition of two single plane waves going in opposite directions, with a much reduced amplitude compared to Δ_0.

We note that in the weak coupling limit, a sonoidal solution of the order parameter for the BdG equations was found analytically if one linearizes the single particle spectrum at the Fermi surface [94,95], which gives qualitatively the same behavior as shown in Fig. 7.

C. Phase diagram from BdG solutions

We examine the phase diagram obtained by the single-plane-wave approximation (Fig. 5). For this purpose, we compare the results of the spin polarization versus the chemical potential difference, as predicted respectively by the self-consistent BdG formalism and the single-plane-wave approximation or the FF solution. As shown in Fig. 8, the self-consistent prediction agrees very well with that of the FF solution at a large chemical potential difference. However, approaching to the BCS-FFLO transition point, they differ largely. The quick fall of the spin polarization in the self-consistent BdG indicates strongly the existence of a FFLO state with an arbitrary small spin polarization. As the spin polarization is a first-order derivative of the energy, this is a solid evidence for the smooth transition from the BCS state to the FFLO state. We therefore conclude that although the single-plane-wave approximation gives a reasonable description at the large chemical potential difference, it does not predict the correct phase transition between BCS and FFLO states.
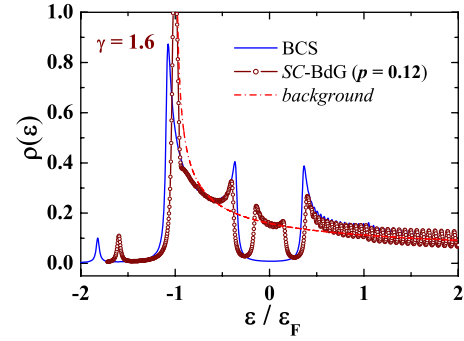

FIG. 9. (Color online) Local fermionic density of states of a uniform polarized Fermi gas at an interaction strength $\gamma=1.6$, calculated using the self-consistent BdG equations.

We may extract the critical behavior at the transition point by numerically analyzing the self-consistent data. Assuming a power-law dependence of the spin polarization on the chemical potential difference, $p \propto (\delta\mu - \delta\mu_c)^{\alpha}$, we find that $\alpha \simeq 0.4$, in good agreement with a nonperturbative bosonization prediction [93], $\alpha=0.5$. The small discrepancy may be caused by the use of a finite length L, which becomes increasingly inefficient due to the divergent correlation length towards the transition point.

D. Local fermionic density of states

We finally calculate the local density of states in the self-consistent BdG solutions, which is given by

$$\rho_{\uparrow}(x,\epsilon) = \sum_{\eta} u_{\eta}^2(x)\delta(\epsilon - E_{\eta}), \qquad (4.49)$$

$$\rho_{\downarrow}(x,\epsilon) = \sum_{\eta} v_{\eta}^2(x)\delta(\epsilon + E_{\eta}). \qquad (4.50)$$

In Fig. 9, we show how the local density of states at origin evolves with increasing the spin polarization p from zero to 0.12. Here a small spectral broadening of about $0.02\epsilon_F$ has been used to regularize the delta function. We find again a nonzero density of states at the Fermi surface for a polarized Fermi gas, contributed by the midgap states. As a result, the original BCS gap of a width $2\Delta_0$ is split into two subgaps with a much smaller width.

V. EXACT BETHE ANSATZ SOLUTION IN A HOMOGENEOUS GAS

The validity of mean-field results in 1D is not immediately clear, as pair fluctuations become increasingly important in lower dimensions. Fortunately, without the trap the Hamiltonian (2.1) of a free polarized Fermi gas is exactly soluble, using the Bethe ansatz technique [86,87]. We therefore can use the exact solution as a benchmark to test the validity of various mean-field approaches.

In the thermodynamic limit, the ground state of a homogeneous gas with fixed linear densities $n_{\uparrow}$ and $n_{\downarrow}$ may be obtained from a set of Gaudin integral equations [87],

$$\pi\rho(k) = \frac{1}{2} - \int_{-B}^{B} \frac{c'\sigma(\Lambda)d\Lambda}{c'^2 + (k-\Lambda)^2}, \tag{5.1}$$

$$\pi\sigma(\Lambda) = 1 - \int_{-Q}^{Q} \frac{c'\rho(k)dk}{c'^2 + (\Lambda-k)^2} - \int_{-B}^{B} \frac{c\sigma(\Lambda')d\Lambda'}{c^2 + (\Lambda-\Lambda')^2}, \tag{5.2}$$

and

$$\epsilon_{gs} = \frac{\hbar^2}{2m} \left(\int_{-Q}^{Q} k^2\rho(k) + \int_{-B}^{B} 2\Lambda^2\sigma(\Lambda) - \frac{n_\downarrow c^2}{2} \right), \tag{}$$

$$n_\uparrow - n_\downarrow = \int_{-Q}^{Q} \rho(k)dk, \tag{5.3}$$

$$n_\downarrow = \int_{-B}^{B} \sigma(\Lambda)d\Lambda, \tag{5.4}$$

where ϵ_{gs} is the ground state energy density, the couplings $c=n\gamma$ and $c'=c/2$. The functions $\rho(k)$ and $\sigma(\Lambda)$ are, respectively, the quasimomentum distributions with the cutoff rapidities Q and B to be determined by the normalization condition for $\delta n = n_\uparrow - n_\downarrow$ and $n_\downarrow$. The last term in ϵ_{gs} is simply the contribution from $n_\downarrow$ paired two-fermion bound states with binding energy

$$\epsilon_b = \frac{\hbar^2 c^2}{4m} = \frac{\hbar^2}{ma_{1D}^2}. \tag{5.5}$$

The chemical potential and the chemical potential difference can be obtained by $\mu = \partial\epsilon_{gs}/\partial n$ and $\delta\mu = \partial\epsilon_{gs}/\partial\delta n$, respectively.

A. Gaudin solutions

The Gaudin integral equations must be solved numerically for a general spin polarization $p = \delta n/n$. To do so, we introduce two new variables $x = k/Q$ and $y = \Lambda/B$, and rewrite the quasimomentum distribution functions,

$$g_c(x) = \rho(Qx) = \rho(k), \tag{5.6}$$

$$g_s(y) = \sigma(By) = \sigma(\Lambda). \tag{5.7}$$

Further, the two cutoff rapidities may be represented by, respectively, $Q = n\gamma/\lambda_c$ and $B = n\gamma/\lambda_s$. In such a way, the Gaudin integral equations can be rewritten in a dimensionless form,

$$g_c(x) = \frac{1}{2\pi} - \int_{-1}^{+1} \frac{g_s(y)/(2\pi\lambda_s)}{\frac{1}{4} + \left(\frac{x}{\lambda_c} - \frac{y}{\lambda_s}\right)^2} dy, \tag{5.8}$$

$$g_s(x) = \frac{1}{\pi} - \int_{-1}^{+1} \frac{g_c(y)/(2\pi\lambda_c)}{\frac{1}{4} + \left(\frac{x}{\lambda_s} - \frac{y}{\lambda_c}\right)^2} dy - \int_{-1}^{+1} \frac{g_s(y)/(\pi\lambda_s)}{1 + \left(\frac{x-y}{\lambda_s}\right)^2} dy, \tag{5.9}$$

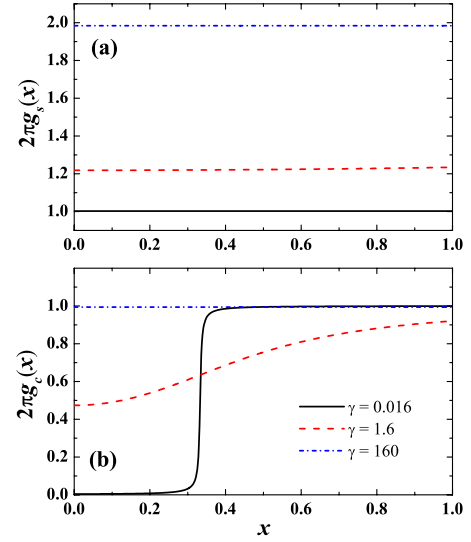together with the normalization conditions,

FIG. 10. (Color online) Gaudin solution for the dimensionless quasimomentum distributions at a spin polarization $p=0.5$ and at several interaction couplings as indicated.

$$\lambda_c = \frac{\gamma}{p} \int_{-1}^{+1} g_c(x)dx, \tag{5.10}$$

$$\lambda_s = \frac{2\gamma}{1-p} \int_{-1}^{+1} g_s(x)dx. \tag{5.11}$$

Numerically, the dimensionless integral equations have been solved by decomposing the integrals on a grid with N points $\{x_i; x_i \in [-1, +1]\}$. In detail, we start from a set of trial distributions $g_c^{(0)}(x_i)$ and $g_s^{(0)}(x_i)$, and the corresponding parameters of $\lambda_c^{(0)}$ and $\lambda_s^{(0)}$. Following the standard method for the integrals [107], we obtain $g_c(x_i)$ and $g_s(x_i)$. Let $g_c^{(1)}(x_i) = \alpha g_c^{(0)}(x_i) + (1-\alpha)g_c(x_i)$ and $g_s^{(1)}(x_i) = \alpha g_s^{(0)}(x_i) + (1-\alpha)g_s(x_i)$ (where α is a positive real number between 0 and 1, depending on the value of the spin polarization) be the new trial distributions, and update $\lambda_c^{(1)}$ and $\lambda_s^{(1)}$ accordingly. Repeat the above procedure until $g_c(x_i)$ and $g_s(x_i)$ agree with their trial distributions within a certain range. Then, the energy density

$$\epsilon_{gs} = \frac{\hbar^2 n^3}{2m} e(\gamma, p) - n_\downarrow \epsilon_b \tag{5.12}$$

is calculated by

$$e(\gamma, p) = \frac{\gamma^3}{\lambda_c^3} \int_{-1}^{+1} x^2 g_c(x)dx + \frac{\gamma^3}{\lambda_s^3} \int_{-1}^{+1} 2x^2 g_s(x)dx. \tag{5.13}$$

We find that this iterative method for solving the Gaudin integral equations is very stable. The chemical potential and chemical potential difference can also be calculated accurately by a numerical derivative.

For an illustrative purpose, we plot in Fig. 10 the quasimomentum distribution functions $g_s(x)$ [Fig. 10(a)] and $g_c(x)$ [Fig. 10(b)] at a spin polarization $p=0.5$ for three interaction
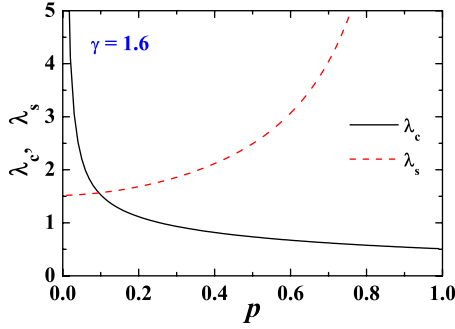
FIG. 11. (Color online) Gaudin solution for the dimensionless parameters λ_c and λ_s, as a function of the spin polarization at an interaction strength $\gamma = 1.6$.

strengths as indicated. As $g_s(x)$ and $g_c(x)$ are both even functions, we show only the part with a positive x. For a large interaction strength, they approach $1/\pi$ and $1/(2\pi)$, respectively. On the other hand, for a weak interaction, $g_s(x)$ reduces to $1/(2\pi)$ and $g_c(x)$ jumps from zero to $1/(2\pi)$ at a certain value of x.

At $\gamma = 1.6$ the dimensionless parameters λ_c and λ_s as a function of the spin polarization are shown in Fig. 11. They diverge, respectively, as $1/p$ and $1/(1-p)$ when the spin polarization goes to 0 or 1.

B. Analytic results in limiting cases

The asymptotic behavior of the Gaudin solution may be obtained in the strongly and weakly interacting limits. For a strongly interacting gas, for which the dimensionless coupling constant $\gamma \gg 1$, the parameters λ_c and λ_s are sufficiently large. Therefore, the integrals in the Gaudin equations become extremely small. Hence, the quasimomentum distributions $g_c(x)$ and $g_s(x)$ are essentially constant. Expanding to the order $1/\gamma^3$, we find that,

$$g_c(x) = \frac{1}{2\pi} - \frac{1-p}{\pi\gamma} + o\left(\frac{1}{\gamma^3}\right), \tag{5.14}$$

$$g_s(x) = \frac{1}{\pi} - \frac{1+3p}{2\pi\gamma} + o\left(\frac{1}{\gamma^3}\right). \tag{5.15}$$

It is then straightforward to show that to leading order in $1/\gamma$,

$$e(\gamma, p) \simeq \frac{\pi^2(1-p)^3}{48} + \frac{\pi^2 p^3}{3}, \tag{5.16}$$

$$\mu \simeq -\frac{\epsilon_b}{2} + \frac{\hbar^2 n^2}{2m}\frac{\pi^2(1-p)^2}{16}, \tag{5.17}$$

$$\delta\mu \simeq \frac{\epsilon_b}{2} - \frac{\hbar^2 n^2}{2m}\frac{\pi^2(1-p)^2}{16} + \frac{\hbar^2 n^2}{2m}\pi^2 p^2. \tag{5.18}$$

Recalling that $n_\downarrow = n(1-p)/2$, the chemical potential, as well as the first two terms on the right-hand side of the chemical

potential difference, coincide in magnitude with the chemical potential of a Tonks-Girardeau bosonic gas of paired $n_\downarrow$ dimers [107], which is fermionized due to strong attractions. The third term in the chemical potential difference, on the other hand, is equal to the chemical potential of residual unpaired $n_\uparrow - n_\downarrow$ fermions. Therefore, in the strong coupling regime the polarized gas behaves like an incoherent mixture of a molecular Bose gas and a fully polarized single-species Fermi gas.

The analytic derivation in the weak coupling limit $\gamma \ll 1$ is much more subtle since the quasimomentum distribution $g_c(x)$ contains a sharp jump whose width ($\sim \gamma$) is extremely small, as shown in Fig. 10(b) for $\gamma = 0.016$. However, as a leading approximation, we may take $g_c(x)$ as a step function. It is then easy to show that ($\gamma \ll \max\{p, 1-p\}$),

$$g_c(x) = \begin{cases} 0, & |x| < (1-p)/(1+p), \\ 1/(2\pi), & |x| > (1-p)/(1+p), \end{cases} \tag{5.19}$$

$$g_s(x) = 1/(2\pi). \tag{5.20}$$

As a result, the ground state energy density and the chemical potentials are given by

$$e(\gamma, p) \simeq \frac{\pi^2}{12}(1 + 3p^2) - \frac{\gamma}{2}(1 - p^2), \tag{5.21}$$

$$\mu \simeq \frac{\hbar^2 n^2}{2m}\frac{\pi^2}{4}(1 + p^2) + \frac{\hbar^2 n^2}{2m}\gamma, \tag{5.22}$$

$$\delta\mu \simeq \frac{\hbar^2 n^2}{2m}\frac{\pi^2}{2}p + \frac{\hbar^2 n^2}{2m}\gamma p, \tag{5.23}$$

where the first term on the right-hand side corresponds to an ideal polarized gas, while the second term arises from the mean-field Hartree-Fock interactions. We note that a nonperturbative term of order $\gamma^2 \ln \gamma$ will occur if one improves the quasimomentum distribution functions by explicitly taking into account the width of the jump in $g_c(x)$.

C. Mean-field approaches versus exact solutions

We are now ready to verify the accuracy of the mean-field approaches. In Figs. 12 and 13, we compare the energy and chemical potentials of the exact Gaudin solutions with that from mean-field calculations, with either a single-plane-wave-like (labeled as "FF") or a self-consistently determined (denoted by "SC-BdG") order parameter. For comparison, the energy of an ideal polarization gas is also shown. For a moderate interaction coupling $\gamma = 1.6$, we find a reasonable agreement. The residual discrepancy could be ascribed to pair fluctuations, which are small but not negligible. We have also checked that the agreement becomes increasingly better (as expected), with decreasing interaction strength. With these observations, we therefore confirm the validity of the mean-field theories for the weakly and moderately interacting regimes.

On the other hand, the good agreement between the Gaudin solutions and the mean-field results suggests strongly
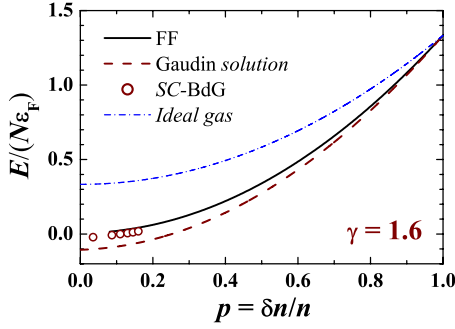
FIG. 12. (Color online) Comparison of the mean-field energy to the exact results obtained from the Bethe ansatz solution at an interaction strength $\gamma = 1.6$. For a reference, we plot also the energy of an ideal polarized gas. Presumably, the small discrepancy between the mean-field and exact results is due to the pair fluctuation effects.

that the partially polarized solution found in the exact Bethe ansatz method is of FFLO character. We note that a calculation of the nonlocal pair correlation functions in the exact solution would be very useful to unambiguously determine its structure. However, this is extremely difficult due to the complicated ground state wave functions from the Bethe ansatz.

D. Quantitative phase diagram of a homogeneous polarized Fermi gas

Gathering all the information from the Gaudin integral solutions and the two mean-field results, we arrive at a quantitative phase diagram for a homogeneous polarized Fermi gas [85,92]. For a given interaction strength the chemical potential difference takes values between two thresholds, $\delta\mu_{c,p=0}$ and $\delta\mu_{c,p=1}$, as indicated by arrows in Fig. 13 for $\gamma = 1.6$. Below the first threshold $\delta\mu_{c,p=0}$, the gas persists in the BCS-like superfluid state with zero polarization (SF), while above the second critical value $\delta\mu_{c,p=1}$, a fully polarized normal state appears (N). In between, a superfluid state with finite polarization (SF_P) is favored. As stated earlier, the SF_P has a FFLO structure in character. Physically $\delta\mu_{c,p=0}$ is the
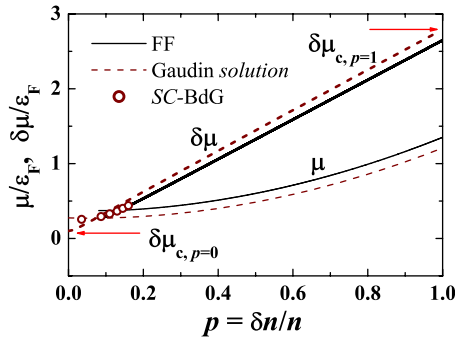

FIG. 13. (Color online) Comparison of the mean-field chemical potentials to the exact results obtained from the Bethe ansatz solution at an interaction strength $\gamma = 1.6$. The arrows point to two critical chemical potential differences, between which a polarized superfluid exists.
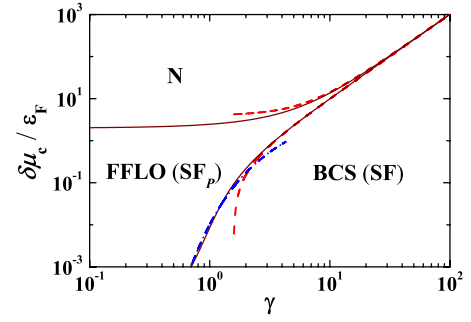

FIG. 14. (Color online) Phase diagram of a one-dimensional homogeneous spin-polarized Fermi gas. The dotted-dashed line refers to the asymptotic expression of the critical chemical potential difference in the weak coupling limit, i.e., Eq. (5.27), while the two dashed lines are, respectively, the strong-coupling expansion of the critical chemical potential difference, as described in Eqs. (5.24) and (5.25).

energy cost required to break spin-singlet pairs in unpolarized superfluid, i.e., the spin gap, while $\delta\mu_{c,p=1}$ is also associated with the pair-breaking (for the last pair), but is enhanced due to the Pauli repulsion from existing fermions. The dependence of $\delta\mu_{c,p=0}$ and $\delta\mu_{c,p=1}$ on the parameter γ is reported in Fig. 14, constituting a homogeneous phase diagram.

The behavior of the critical chemical potential difference in the weak and strong coupling limits may be worked out analytically. In the strongly interacting regime of $\gamma \to \infty$, from its asymptotic expression (5.18) we find that,

$$\delta\mu_{c,p=0} \simeq \frac{\epsilon_b}{2} - \frac{\hbar^2 n^2}{2m}\frac{\pi^2}{16}, \qquad (5.24)$$

$$\delta\mu_{c,p=1} \simeq \frac{\epsilon_b}{2} + \frac{\hbar^2 n^2}{2m}\pi^2. \qquad (5.25)$$

While in the weakly interacting limit of $\gamma \to 0$, only $\delta\mu_{c,p=1}$ can be determined from the weak coupling expression (5.23),

$$\delta\mu_{c,p=1} \simeq \frac{\hbar^2 n^2}{2m}\left(\frac{\pi^2}{2} + \gamma\right), \qquad (5.26)$$

as the validity of the equation is restricted to $\gamma \ll \max\{p, 1-p\}$. The determination of $\delta\mu_{c,p=0}$ as $\gamma \to 0$ turns out to be very difficult. Fortunately, it has been studied by Krivnov and Ovchinnikov [88], and Fuchs, Recati, and Zwerger [106] in detail. Here we only quote their result,

$$\delta\mu_{c,p=0} \simeq \frac{\hbar^2 n^2}{2m}2\sqrt{\pi\gamma}\exp\left(-\frac{\pi^2}{2\gamma}\right). \qquad (5.27)$$

This predicts the same exponent $-\pi^2/(2\gamma)$ as the BCS mean-field theory. However, there is a different power-law dependence of the prefactor on the dimensionless coupling constant. i.e., it has an extra $\sqrt{\gamma}$ factor. In Fig. 14, we plot these analytic predictions using dashed and dotted-dashed lines. They are in excellent agreement with the exact numerical results in the regions where they are valid.
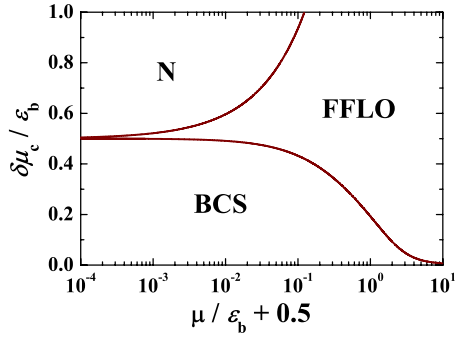
FIG. 15. (Color online) Same phase diagram as in Fig. 12, but plotted here in the plane of the chemical potential and the chemical potential difference. Note that the chemical potential difference is in units of the binding energy, so that the diagram is particularly useful for the case with a fixed interaction strength, but varying densities.

For a later reference, in Fig. 15 we reconstruct the phase diagram in the plane of the chemical potential and the chemical potential difference. Both of them are measured in units of the binding energy. It is clear that in the strong coupling limit, the two critical chemical potential differences converge to one-half of the binding energy, and the phase space for the FFLO states therefore becomes much narrower.

VI. SELF-CONSISTENT BdG APPROACH IN A HARMONIC TRAP

To make a quantitative contact with the on-going experiments, it is crucial to take into account the trapping potential that is necessary to prevent the atoms from escaping. In this section we turn to describe a 1D polarized gas in harmonic traps, using the mean-field BdG equations.

With the trap $V_{\mathrm{trap}}(x) = m\omega^2 x^2/2$, the BdG formalism is essentially the same as that under a periodic boundary condition, except a few modifications: (1) First, one must replace everywhere the chemical potential μ by a local potential $\mu - V_{\mathrm{trap}}(x)$. (2) Second, to solve the BdG equation, it is convenient to use the eigenfunctions of the harmonic trap,

$$\varphi_n(x) = A_n H_n\left(\frac{x}{a_{ho}}\right)\exp\left(-\frac{x^2}{2a_{ho}^2}\right), \quad (6.1)$$

as the set of the expanding basis. Here $H_n(x)$ is the Hermite polynomial with an order n, $a_{ho} = [\hbar/(m\omega)]^{1/2}$ is the characteristic harmonic oscillator length, and $A_n = \sqrt{1/(\pi^{1/2}2^n n!)}$ is the normalization factor for single particle eigenfunctions. (3) Third, for the convenience of the numerical calculations, it is better to take the trap units, i.e., $m=\hbar=\omega=1$, so that the length and energy will be measured in units of the characteristic harmonic oscillator length a_{ho} and $\hbar\omega$, respectively. (4) Finally, in the presence of the trap, there is no restriction for the initial guess of the order parameter. We may then initialize the order parameter by choosing some random values.

We have performed a calculation for a gas with $N=128$ fermions in traps at zero temperature. The Fermi energy under the unpolarized condition is $E_F = (N/2)\hbar\omega = 64\hbar\omega$. We therefore take a cutoff energy $E_c = 6E_F = 384\hbar\omega$ and keep up
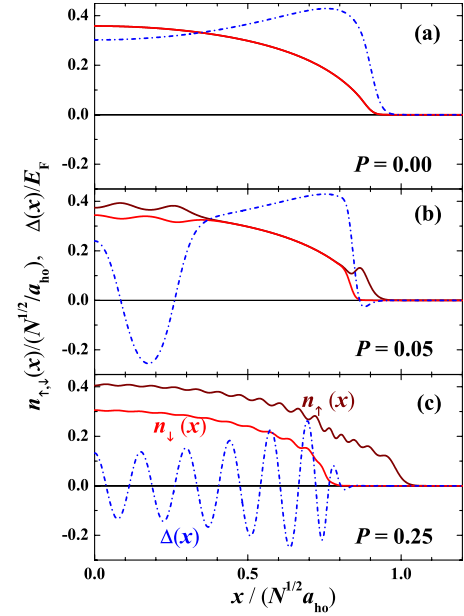

FIG. 16. (Color online) Density profiles (solid lines) and order parameters (dotted-dashed lines) of a trapped Fermi gas at several total spin polarizations as indicated. The dimensionless coupling constant at the trap center γ_0 is 1.6. With increasing the total spin polarization, the FFLO enters gradually at center, leading to two phase separation phases.

to $6N=768$ single particle eigenfunctions. These parameters are already very large to ensure the accuracy of the calculations. As mentioned earlier, we use the dimensionless coupling parameter at the trap center, $\gamma_0 = \pi a_{ho}/(N^{1/2}a_{1D})$, to characterize the interaction. In Fig. 16, we present the BdG results for the density profiles (solid lines) and the order parameter (dotted-dashed lines) at a moderate interaction strength $\gamma_0 = 1.6$ for three total spin polarizations as indicated.

For a pure BCS superfluid with zero polarization [Fig. 16(a)], the spin-up and spin-down density profiles coincide, and decrease monotonically as expected. However, the order parameter is nonmonotonic: it increases slowly up to the boundary of the trap, and then drops to zero very rapidly. A maximum at the trap edge then arises in the order parameter, in marked contrast to the 3D cases, where the order parameter decreases monotonically. This maximum is due to the low dimensionality of the gas. Recall that the BCS prediction of the gap for a uniform gas $\Delta_{\mathrm{BCS}} \simeq 8\epsilon_F \exp[-\pi^2/(2\gamma)]$. At the local position x, $\epsilon_F \propto n^2(x)$, while $\gamma = 2/[a_{1D}n(x)]$. As a result, the position-dependent order parameter is given by

$$\Delta_{\mathrm{BCS}}(x) \propto n^2(x)\exp\left(-\frac{\pi^2}{4}a_{1D}n(x)\right), \quad (6.2)$$

which is a product of $n^2(x)$ and of an exponent. These two parts decrease and increase, respectively, towards the trap edge. Particularly, the increase of the exponent is due to the increase of the effective interactions, which becomes much larger with decreasing density. Therefore their interplay should result in a maximum. In general, the exponent is
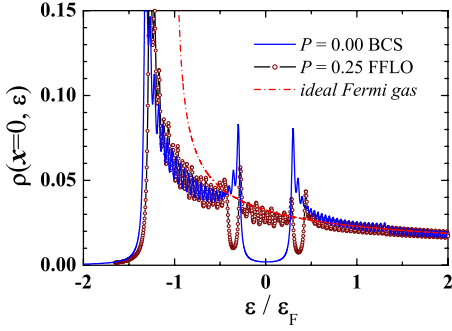
FIG. 17. (Color online) Local fermionic density of states of a trapped polarized Fermi gas at an interaction strength $\gamma_0 = 1.6$. The remarkable two-energy-gap structure is robust in the trap environment.

dominant, thereby the sharp decrease or the maximum of $\Delta_{\text{BCS}}(x)$ occurs at the trap edge for a moderate local density.

With increasing total spin polarization, the order parameter starts to oscillate at the trap center, suggesting the entry of FFLO-type states at center. Correspondingly, the spin-up and spin-down density profiles are no longer the same. For a small total spin polarization [Fig. 16(b)], the oscillation of the order parameter is restricted at the trap center, and the ordinary BCS order parameter still persists at the edge. As a consequence, we find a phase separation phase consisting of a FFLO state at the trap center and a standard BCS state outside. There is also a very small region with a weak oscillation of the order parameter, occurring exactly at the trap boundary. Presumably, it is a finite size effect. As we shall see later, the resulting normal cloud at the boundary is an artifact of the mean-field theory, which will break down at sufficiently small densities or large interactions.

Increasing further the spin polarizations [Fig. 16(c)], the oscillations of the order parameter penetrate the whole cloud. We find then another phase separation phase, with an interior core of a FFLO superfluid phase and an outer shell of the normal component. Therefore, there should be a critical total spin polarization, P_c, that separates the two phase separation phases. The periodicity of the oscillations in the FFLO phase can be estimated, and we find a reasonable agreement with the single-plane-wave estimation for q if we treat the gas as locally homogeneous at the trap center.

The validity of the mean-field BdG calculations in the trap environment will be commented on later, by comparing the mean-field density profiles with that obtained from the exact Gaudin solution and the local density approximation. The physical reason for the two phase separation phases and the value of P_c, as well as the small oscillations in the density profiles, will also be addressed.

Finally, we study the local fermionic density of the state in the trap. In Fig. 17, we report the density of states at the trap center for a BCS superfluid (a) and a FFLO superfluid (b). In the presence of the trap, we find that the essential feature of a two-energy-gap structure in the FFLO state is still apparent. This may provide us with a useful experimental signature to detect indirectly the FFLO states.

VII. ASYMPTOTICALLY EXACT GAUDIN SOLUTIONS IN A HARMONIC TRAP

For a large number of fermions, a useful method to account for external trapping of potential traps is to use the local density approximation [85,92]. Together with the Gaudin solution for the homogeneous equation of states of a polarized Fermi gas, this gives an asymptotically exact result as long as $N \gg 1$. This condition is readily satisfied in the on-going 1D experiment, where the typical number of atoms $N \sim 100$.

The main idea of the local density approximation is that the system can be treated locally as infinite matter with a local chemical potential. We then partition the cloud into many cells in which the number of fermions is much greater than unity. Provided that the variation of the trap potential across the cell is small compared with the local Fermi energy, the interface effects are negligible [75,80]. Qualitatively, the interface energy should scale like $N^{-1/d}$ compared to the total energy, where d is the dimensionality.

In detail, the local density approximation (LDA) amounts to determining the chemical potential $\mu_g = (\mu_{\uparrow g} + \mu_{\downarrow g})/2$ and the chemical potential difference $\delta\mu_g = (\mu_{\uparrow g} - \mu_{\downarrow g})/2$ of the inhomogeneous gas from the local equilibrium conditions,

$$\mu_\uparrow[n(x), p(x)] + \frac{1}{2} m\omega^2 x^2 = \mu_{\uparrow g}, \tag{7.1}$$

$$\mu_\downarrow[n(x), p(x)] + \frac{1}{2} m\omega^2 x^2 = \mu_{\downarrow g}, \tag{7.2}$$

and the normalization conditions,

$$N = \int_{-\infty}^{+\infty} n(x)\,dx, \tag{7.3}$$

$$NP = \int_{-\infty}^{+\infty} n(x)p(x)\,dx, \tag{7.4}$$

where $n(x)$ and $p(x)$ are, respectively, the total linear density and the local spin polarization, and P is the total spin polarization. We have used a subscript "g" to denote the global chemical potentials.

To solve these equations, we rewrite the chemical potentials in the form

$$\mu_\uparrow[n(x), p(x)] = \frac{\hbar^2}{2m} n^2(x) \bar{\mu}_\uparrow[\gamma(x), p(x)], \tag{7.5}$$

$$\mu_\downarrow[n(x), p(x)] = \frac{\hbar^2}{2m} n^2(x) \bar{\mu}_\downarrow[\gamma(x), p(x)], \tag{7.6}$$

where $\bar{\mu}_\sigma$ are the reduced chemical potentials, depending on the dimensionless coupling constant and local spin polarization only. Further, it is convenient to rescale the chemical potentials coordinate and total linear density into a dimensionless form, i.e.,

$$\bar{\mu}_{\sigma g} = \frac{\mu_{\sigma g}}{\epsilon_b}, \tag{7.7}$$

$$\bar{x} = \frac{a_{1D}x}{a_{ho}^2}, \tag{7.8}$$

$$\bar{n} = na_{1D}. \tag{7.9}$$

Then the local equilibrium equations and the normalization equations can be rewritten as

$$\frac{\bar{n}^2(\bar{x})}{2}\bar{\mu}_\uparrow[\gamma(\bar{x}), p(\bar{x})] + \frac{\bar{x}^2}{2} = \bar{\mu}_{\uparrow g}, \tag{7.10}$$

$$\frac{\bar{n}^2(\bar{x})}{2}\bar{\mu}_\downarrow[\gamma(\bar{x}), p(\bar{x})] + \frac{\bar{x}^2}{2} = \bar{\mu}_{\downarrow g}, \tag{7.11}$$

and

$$\frac{1}{\pi^2\gamma_0^2} = \int_{-\infty}^{+\infty} \bar{n}(\bar{x})d\bar{x}, \tag{7.12}$$

$$\left(\frac{1}{\pi^2\gamma_0^2}\right)P = \int_{-\infty}^{+\infty} \bar{n}(\bar{x})p(\bar{x})d\bar{x}, \tag{7.13}$$

where $\gamma(\bar{x}) = 2/\bar{n}(\bar{x})$. The terms on the left-hand side of the last two equations emphasize that the properties of the cloud rely on two dimensionless parameters, γ_0 and P. In particular, the coupling constant in a trap is controlled by γ_0, where $\gamma_0 \ll 1$ corresponds to weak coupling, while $\gamma_0 \gg 1$ corresponds to the strongly interacting regime.

The numerical procedure for the local density approximation is straightforward. For given parameters γ_0 and P, and initial guess for $\bar{\mu}_{\sigma g}$, we invert the dimensionless local equilibrium equations to find $\gamma(\bar{x})$ and $p(\bar{x})$. The chemical potentials $\bar{\mu}_{\sigma g}$ are then adjusted slightly to enforce number conservation, giving a better estimate for the next iterative step. The iteration is continued until the number conditions are satisfied within a certain range.

A. Density profiles: LDA vs BdG

In Fig. 18, we give the density profiles obtained from the local density approximation using dashed lines. For comparison, we show also the results of the BdG solutions. Apart from a negligible difference at the trap boundary (due to a breakdown of mean-field theory), we find a good agreement. This becomes even better as the total spin polarization increases. In particular, the two phase separation phases found in the BdG calculations are evident.

The appearance of the phase separation phases is easy to understand. Within the local density approximation, the local chemical potential $\mu(x)$ decreases parabolically away from the center of the trap while the local chemical potential difference $\delta\mu(x)$ stays constant. It is then evident from Fig. 15 that with a nonzero spin polarization we always have a polarized FFLO superfluid at the trap center where the local chemical potential (or interaction parameter) is large (or small). Away from the center with decreasing local chemical potential, the gas enters into either an unpolarized BCS superfluid or a fully polarized normal cloud, depending on
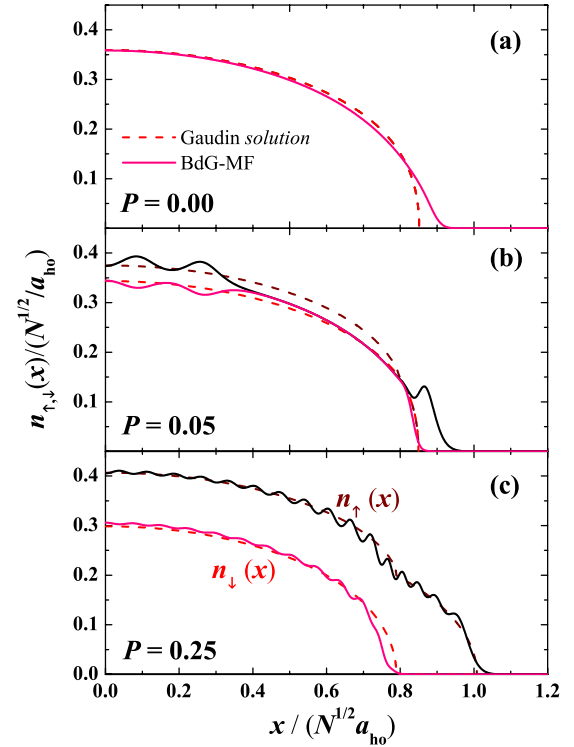

FIG. 18. (Color online) Density profiles of a trapped gas, calculated by the exact Gaudin solution and the local density approximation, are shown for several spin polarizations as indicated. For comparison, we plot also the self-consistent mean-field BdG predictions. They are in reasonable agreement at the center. A discrepancy occurs at the trap edge, where for small polarization, the approximate BdG calculation overestimates the size of the unpolarized BCS shell.

whether the chemical potential difference is smaller than one-half of the binding energy or not. Thus, there is a critical chemical potential difference $\delta\mu_c \equiv \epsilon_b/2$ that separates the inhomogeneous system into two phase separation states: a mixture of a polarized superfluid core and an unpolarized superfluid shell (FFLO-BCS), or a coexistence of a polarized superfluid at the center and a fully polarized normal gas outside (FFLO-BCS).

It should be noted that the former phase separation phase is exotic, as the BCS-like superfluid state occurs at the edge of the trap, in marked contrast to the 3D case. This is caused by the peculiar effects of low dimensionality, for which the gas becomes more nonideal with decreasing 1D density towards the edge of the trap, and hence the energy required to break the pairs approaches $\epsilon_b/2$ from below. As $\delta\mu_g < \epsilon_b/2$, there should be a fully paired region once the local critical chemical potential $\delta\mu_{c,p=0} > \delta\mu_g$, i.e., the BCS-like superfluid.

Though the basic feature of the BdG results is well reproduced by the local density approximation calculations, we note that there are still some discrepancies that merit careful examination. First, with decreasing the density the mean-field theory seems to fail at the trap edge, as shown in Figs. 18(a) and 18(b). For a small polarization $P = 0.05$ [Fig. 18(b)], a notable discrepancy thus occurs at the trap edge.
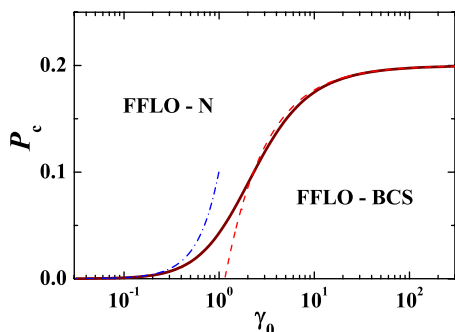
FIG. 19. (Color online) Phase diagram of a one-dimensional trapped spin-polarized Fermi gas. The dashed line and dotted-dashed line are the asymptotic results for the critical spin polarization in the strongly and weakly interacting regimes, respectively.

The very small unpolarized BCS shell, roughly from $0.80N^{1/2}a_{ho}$ to $0.85N^{1/2}a_{ho}$ as predicted by the LDA calculation, becomes strongly overestimated by the mean-field calculation. Second, there are small oscillations in the BdG density profiles. Presumably, these oscillations, observed also in a box with periodic boundary conditions, are either due to the presence of the FFLO states or due to a finite size effect. Considering the absence of the true long-range order in 1D, we prefer the latter interpretation, and regard them as the Friedel oscillations caused by the residual unpaired atoms. To check this point, in the BdG calculations we have varied the total number of fermions, while keeping other parameters invariant. The oscillations become less pronounced with increasing numbers of atoms. We emphasize that in the ongoing experiments, the total number of atoms is about 100. Therefore, the oscillations in the density profiles could be observed experimentally. However, they may hardly be considered as a fundamental signature of the presence of the FFLO states.

B. Phase diagram of a polarized Fermi gas in traps

We may determine numerically the critical spin polarization P_c from the critical chemical potential difference $\delta\mu_c = \epsilon_b/2$. In Fig. 19, we present P_c as a function of the interaction coupling constant γ_0, giving rise to a phase diagram of the inhomogeneous polarized 1D Fermi gas [85,92]. Again, the asymptotic behavior of P_c may be computed analytically in the weak and strong coupling limits. These are shown in the figure using a dashed line and a dotted-dashed line, respectively.

Consider first a strongly interacting gas with $\gamma(x) \geq \gamma_0 \gg 1$. Using the asymptotic expression for the chemical potential and chemical potential difference, the rescaled local equilibrium equations can be rewritten as

$$-\frac{1}{2} + \frac{\pi^2 \bar{n}^2(\bar{x})}{32}[1 - p(\bar{x})]^2 + \frac{\bar{x}^2}{2} = \bar{\mu}_g,$$

$$\frac{1}{2} + \frac{\pi^2 \bar{n}^2(\bar{x})}{32}A[p(\bar{x})] + \frac{\pi^2 \bar{n}^3(\bar{x})}{4}B[p(\bar{x})] = \delta\bar{\mu}_g, \quad (7.14)$$

where $A[p(\bar{x})] = -1 + 2p(\bar{x}) + 15p^2(\bar{x})$ and $B[p(\bar{x})] = -p(\bar{x})/4 + 9p^2(\bar{x})/2 - 67p^3(\bar{x})/12$. Note that in this limit $\bar{n}(\bar{x}) \ll 1$. In

the rescaled units, the critical chemical potential difference $\delta\bar{\mu}_g$ is exactly $1/2$. Therefore, if we consider up to $A[p(\bar{x})]$ only in the expansion, we find that the local spin polarization should satisfy

$$15p^2(\bar{x}) + 2p(\bar{x}) - 1 = 0, \quad (7.15)$$

which yields $p(\bar{x}) \equiv 1/5$ and hence the total spin polarization $P_c = 1/5$. The improvement to the next order requires the inclusion of the term $B[p(\bar{x})]$. For this purpose, we assume $p(\bar{x}) = 1/5 - \delta(\bar{x})$, where $\delta(\bar{x}) \ll 1$. The summation of $A[p(\bar{x})]$ and $B[p(\bar{x})]$ terms should be zero at the critical polarization. Thus, to leading order of $\delta(\bar{x})$, we find that,

$$\delta(\bar{x}) = \frac{32}{375}\bar{n}(\bar{x}). \quad (7.16)$$

The density profile $\bar{n}(\bar{x})$ can be determined by using the local equilibrium equation for $\bar{\mu}_g$, which to a good approximation

$$-\frac{1}{2} + \frac{\pi^2}{50}\bar{n}^2(\bar{x}) + \frac{\bar{x}^2}{2} = \bar{\mu}_g. \quad (7.17)$$

Combined with the normalization condition, $\int_{-\infty}^{+\infty}\bar{n}(\bar{x})d\bar{x} = 1/(\pi^2\gamma_0^2)$, we find that

$$\bar{n}(\bar{x}) = \frac{\sqrt{10}}{\pi^2\gamma_0}\left(1 - \frac{5\pi^2\gamma_0^2\bar{x}^2}{2}\right)^{1/2}. \quad (7.18)$$

Therefore, we determine the critical spin polarization using $P_c = \pi^2\gamma_0^2\int_{-\infty}^{+\infty}\bar{n}(\bar{x})p(\bar{x})d\bar{x}$ and find that

$$P_c = \frac{1}{5} - \frac{256}{225\pi^3}\sqrt{\frac{2}{5}}\frac{1}{\gamma_0} = 0.2 - \frac{0.023\,208}{\gamma_0}. \quad (7.19)$$

The consideration in the weak coupling limit is much simpler. In the rescaled units,

$$\delta\bar{\mu}[\bar{n}(\bar{x}), p(\bar{x})] = \frac{\pi^2\bar{n}^2(\bar{x})p(\bar{x})}{4} = \delta\bar{\mu}_g, \quad (7.20)$$

where in this limit $\bar{n}(\bar{x}) \gg 1$. By setting $\delta\bar{\mu}_g = 1/2$, we then obtain

$$p(\bar{x}) = \frac{2}{\pi^2}\frac{1}{\bar{n}^2(\bar{x})}. \quad (7.21)$$

Using again the normalization condition for the total number of atoms, the rescaled (ideal) density profile takes the form

$$\bar{n}(\bar{x}) = \frac{2}{\pi^2\gamma_0}(1 - \pi^2\gamma_0^2\bar{x}^2)^{1/2}. \quad (7.22)$$

Thus, by integrating out $P_c = \pi^2\gamma_0^2\int_{-\infty}^{+\infty}2/[\pi^2\bar{n}(\bar{x})]d\bar{x}$, we find that

$$P_c = \frac{\gamma_0^2}{\pi^2}. \quad (7.23)$$

VIII. CONCLUSIONS AND SOME REMARKS

In conclusion, we have presented a systematic study of an attractive polarized atomic Fermi gas in one dimension, both

in free space and in a harmonic trap. The theoretical approaches include the (asymptotically) exact Bethe ansatz solution and two mean-field approximations: the single-plane-wave approximation for the order parameter and the self-consistent Bogoliubov–de Gennes equations. These useful tools provide us with quantitative phase diagrams in both uniform and harmonic trapped systems. Our main results may be summarized as follows, in response to the theoretical issues raised in the Introduction.

(A) We have clarified the structure of the one-dimensional FFLO states in a uniform gas. For small spin polarization, the FFLO order parameter behaves like a lattice of instantons and anti-instantons, which carry the excess unpaired atoms. For a large spin polarization, the singularity of the instantons merges together. Thus, the form of the order parameter becomes a cosine function, as originally proposed by Larkin and Ovchinnikov [29]. The nodes in the FFLO order parameter lead to a two-energy-gap structure in the local fermionic density of states, which may be experimentally observable using spectroscopic methods.

(B) We have determined the nature of the phase transition from a BCS superfluid state to a FFLO phase. It is a smooth second-order transition. As a consequence, a one-dimensional phase separation does not occur for a homogeneous gas. Turning to the trapped case, we find two exotic phase separation phases. However, these phase separations are simply trap effects.

(C) We have checked the validity of the two mean-field approaches in the weakly or moderately interacting regimes, by comparing the results with the exact or asymptotically exact Bethe ansatz solutions. The mean-field methods are found to provide a useful description in these regimes. In particular, by comparing the equations of state and density profiles, we have shown that the spin polarized superfluid in the Bethe ansatz solution corresponds to an FFLO state, with a real (cosinelike) order parameter. This correspondence, however, does not hold quantitatively in the strongly interacting regime. The Bethe ansatz solutions do not result in any abrupt changes for the polarized superfluid, as the interaction strengths increase from the weak to strong regimes.

Though our study is restricted here to the one-dimensional case, we can still obtain some insight into the phase diagram of a three-dimensional polarized Fermi gas. This is under strong debate at the moment. Two remarks may be in order in this respect.

One key remark is that the FFLO window in three dimensions can be expected to be much larger than that obtained from mean-field calculations with a single-plane-wave assumption for the order parameter. As we have noted, by improving the form of the order parameter to the Larkin and Ovchinnikov (LO) type, $\Delta(\mathbf{x}) \propto \cos[\mathbf{q} \cdot \mathbf{x}]$, Yoshida and Yip have indeed found recently that the FFLO state becomes more stable [54]. Further, the one-dimensional results indicate that one might expect a smooth phase transition from the BCS state to FFLO state in three dimensions, although clearly this needs to be checked with a full three-dimensional calculation.

Another interesting issue concerns the existence of a phase separation in a three dimensional homogeneous polarized gas. From the one-dimensional calculations, we do not find any strong indication for this. Accordingly, the experimentally observed phase separation may simply be understood as a trap effect. We note, however, that the three dimensional strongly interacting BEC limit has no correspondence in the one-dimensional attractive polarized gas [105,106]. It that limit, a homogeneous polarized superfluid, which may be called the Sarma phase, becomes stable [33,34,44]. This phase has a different symmetry from the spatially inhomogeneous FFLO phase. Therefore, there could be another phase intervening between the Sarma phase and the FFLO phase. This may be a possible reason for the observation of phase separation in three dimension. If this exists, we would expect that phase separation for a homogeneous gas would be restricted to the strongly interacting regime near unitarity.

[1] S. Inouye *et al.*, Nature (London) **392**, 151 (1998).

[2] M. Greiner *et al.*, Nature (London) **415**, 39 (2002).

[3] H. Hu, P. D. Drummond, and X.-J. Liu, Nat. Phys. **3**, 469 (2007), and references therein.

[4] A. J. Leggett, *Modern Trends in the Theory of Condensed Matter* (Springer-Verlag, Berlin, 1980).

[5] P. Nozières and S. Schmitt-Rink, J. Low Temp. Phys. **59**, 195 (1985).

[6] J. R. Engelbrecht, M. Randeria, and C. A. R. Sá de Melo, Phys. Rev. B **55**, 15153 (1997).

[7] Y. Ohashi and A. Griffin, Phys. Rev. Lett. **89**, 130402 (2002).

[8] H. Hu, A. Minguzzi, X. J. Liu, and M. P. Tosi, Phys. Rev. Lett. **93**, 190403 (2004).

[9] H. Hu, X.-J. Liu, and P. D. Drummond, Europhys. Lett. **74**, 574 (2006).

[10] C. A. Regal, M. Greiner, and D. S. Jin, Phys. Rev. Lett. **92**, 040403 (2004).

[11] M. W. Zwierlein, C. A. Stan, C. H. Schunck, S. M. F. Raupach, A. J. Kerman, and W. Ketterle, Phys. Rev. Lett. **92**, 120403 (2004).

[12] J. Kinast, S. L. Hemmer, M. E. Gehm, A. Turlapov, and J. E. Thomas, Phys. Rev. Lett. **92**, 150402 (2004).

[13] M. Bartenstein, A. Altmeyer, S. Riedl, S. Jochim, C. Chin, J. H. Denschlag, and R. Grimm, Phys. Rev. Lett. **92**, 203201 (2004).

[14] C. Chin *et al.*, Science **305**, 1128 (2004).

[15] T. Bourdel, L. Khaykovich, J. Cubizolles, J. Zhang, F. Chevy, M. Teichmann, L. Tarruell, S. J. J. M. F. Kokkelmans, and C. Salomon, Phys. Rev. Lett. **93**, 050401 (2004).

[16] J. Kinast *et al.*, Science **307**, 1296 (2005).

[17] M. W. Zwierlein *et al.*, Nature (London) **435**, 1047 (2005).

[18] J. E. Thomas, J. Kinast, and A. Turlapov, Phys. Rev. Lett. **95**, 120402 (2005).

[19] J. K. Chin, Nature (London) **443**, 961 (2006).

[20] L. Luo, B. Clancy, J. Joseph, J. Kinast, and J. E. Thomas, Phys. Rev. Lett. **98**, 080402 (2007).

[21] G. B. Partridge, K. E. Strecker, R. I. Kamar, M. W. Jack, and R. G. Hulet, Phys. Rev. Lett. **95**, 020404 (2005).

[22] M. W. Zwierlein *et al.*, Science **311**, 492 (2006).

[23] M. W. Zwierlein *et al.*, Nature (London) **442**, 54 (2006).

[24] Y. Shin, M. W. Zwierlein, C. H. Schunck, A. Schirotzek, and W. Ketterle, Phys. Rev. Lett. **97**, 030401 (2006).

[25] C. H. Schunck *et al.*, Science **316**, 867 (2007).

[26] G. B. Partridge *et al.*, Science **311**, 503 (2006).

[27] G. B. Partridge, W. Li, Y. A. Liao, R. G. Hulet, M. Haque, and H. T. C. Stoof, Phys. Rev. Lett. **97**, 190407 (2006).

[28] P. Fulde and R. A. Ferrell, Phys. Rev. **135**, A550 (1964).

[29] A. I. Larkin and Y. N. Ovchinnikov, Zh. Eksp. Teor. Fiz. **47**, 1136 (1964) [Sov. Phys. JETP **20**, 762 (1965)].

[30] For a review on the FFLO states, see, for example, R. Casalbuoni and G. Nardulli, Rev. Mod. Phys. **76**, 263 (2004).

[31] H. A. Radovan *et al.*, Nature (London) **425**, 51 (2003); A. Bianchi, R. Movshovich, C. Capan, P. G. Pagliuso, and J. L. Sarrao, Phys. Rev. Lett. **91**, 187004 (2003); C. Martin, C. C. Agosta, S. W. Tozer, H. A. Radovan, E. C. Palm, T. P. Murphy, and J. L. Sarrao, Phys. Rev. B **71**, 020503(R) (2005).

[32] G. Sarma, J. Phys. Chem. Solids **24**, 1029 (1963).

[33] S.-T. Wu and S.-K. Yip, Phys. Rev. A **67**, 053603 (2003).

[34] C.-H. Pao, S.-T. Wu, and S.-K. Yip, Phys. Rev. B **73**, 132506 (2006).

[35] H. Müther and A. Sedrakian, Phys. Rev. Lett. **88**, 252503 (2002).

[36] A. Sedrakian, J. Mur-Petit, A. Polls, and H. Muther, Phys. Rev. A **72**, 013613 (2005).

[37] A. Sedrakian, H. Müther, and A. Polls, Phys. Rev. Lett. **97**, 140404 (2006).

[38] W. V. Liu and F. Wilczek, Phys. Rev. Lett. **90**, 047002 (2003).

[39] P. F. Bedaque, H. Caldas, and G. Rupak, Phys. Rev. Lett. **91**, 247002 (2003).

[40] D. T. Son and M. A. Stephanov, Phys. Rev. A **74**, 013614 (2006).

[41] M. Mannarelli, G. Nardulli, and M. Ruggieri, Phys. Rev. A **74**, 033606 (2006).

[42] K. Yang, e-print arXiv:cond-mat/0508484.

[43] K. Yang, e-print arXiv:cond-mat/0603190.

[44] D. E. Sheehy and L. Radzihovsky, Phys. Rev. Lett. **96**, 060401 (2006).

[45] D. E. Sheehy and L. Radzihovsky, Ann. Phys. (N.Y.) **322**, 1790 (2007).

[46] F. Chevy, Phys. Rev. Lett. **96**, 130401 (2006).

[47] F. Chevy, Phys. Rev. A **74**, 063628 (2006).

[48] H. Hu and X.-J. Liu, Phys. Rev. A **73**, 051603(R) (2006).

[49] X.-J. Liu and H. Hu, Europhys. Lett. **75**, 364 (2006).

[50] H. Hu, X.-J. Liu, and P. D. Drummond, Phys. Rev. Lett. **98**, 060406 (2007).

[51] X.-J. Liu, H. Hu, and P. D. Drummond, Phys. Rev. A **75**, 023614 (2007).

[52] S.-T. Wu, C.-H. Pao, and S.-K. Yip, Phys. Rev. B **74**, 224504 (2006).

[53] C.-H. Pao and S.-K. Yip, J. Phys.: Condens. Matter **18**, 5567 (2006).

[54] N. Yoshida and S.-K. Yip, Phys. Rev. A **75**, 063601 (2007).

[55] M. M. Parish, F. M. Marchetti, A. Lamacraft, and B. D. Simons, Nat. Phys. **3**, 124 (2007).

[56] C. Lobo, A. Recati, S. Giorgini, and S. Stringari, Phys. Rev. Lett. **97**, 200403 (2006).

[57] J. Kinnunen, L. M. Jensen, and P. Törmä, Phys. Rev. Lett. **96**, 110403 (2006).

[58] T. Koponen, J. Kinnunen, J.-P. Martikainen, L. M. Jensen, and P. Törmä, New J. Phys. **8**, 179 (2006).

[59] L. M. Jensen, J. Kinnunen, and P. Törmä, e-print arXiv:cond-mat/0604424.

[60] A. Bulgac, M. McNeil Forbes, and A. Schwenk, Phys. Rev. Lett. **97**, 020402 (2006).

[61] A. Bulgac and M. McNeil Forbes, Phys. Rev. A **75**, 031605(R) (2007).

[62] C.-C. Chien, Q. Chen, Y. He, and K. Levin, Phys. Rev. Lett. **97**, 090402 (2006).

[63] C.-C. Chien, Q. Chen, Y. He, and K. Levin, Phys. Rev. A **74**, 021602(R) (2006).

[64] J. Carlson and S. Reddy, Phys. Rev. Lett. **95**, 060401 (2005).

[65] L. He, M. Jin, and P. Zhuang, Phys. Rev. B **73**, 214527 (2006); **74**, 024516 (2006); **74**, 214516 (2006).

[66] H. Caldas, e-print arXiv:cond-mat/0601148.

[67] H. Caldas, e-print arXiv:cond-mat/0605005.

[68] T.-L. Ho and H. Zhai, J. Low Temp. Phys. **148**, 33 (2007).

[69] Z.-C. Gu, G. Warner, and F. Zhou, e-print arXiv:cond-mat/0603091.

[70] M. Iskin and C. A. R. Sá de Melo, Phys. Rev. Lett. **97**, 100404 (2006).

[71] W. Yi and L.-M. Duan, Phys. Rev. A **73**, 031604(R) (2006).

[72] W. Yi and L.-M. Duan, Phys. Rev. A **73**, 063607 (2006).

[73] W. Yi and L.-M. Duan, Phys. Rev. A **74**, 013610 (2006).

[74] G.-D. Lin, W. Yi, and L.-M. Duan, Phys. Rev. A **74**, 031604(R) (2006).

[75] T. N. De Silva and E. J. Mueller, Phys. Rev. A **73**, 051602(R) (2006).

[76] T. N. De Silva and E. J. Mueller, Phys. Rev. Lett. **97**, 070402 (2006).

[77] M. Haque and H. T. C. Stoof, Phys. Rev. A **74**, 011602(R) (2006).

[78] K. B. Gubbels, M. W. J. Romans, and H. T. C. Stoof, Phys. Rev. Lett. **97**, 210402 (2006).

[79] M. Haque and H. T. C. Stoof, Phys. Rev. Lett. **98**, 260406 (2007).

[80] A. Imambekov, C. J. Bolech, M. Lukin, and E. Demler, Phys. Rev. A **74**, 053626(R) (2006).

[81] J.-P. Martikainen, Phys. Rev. A **74**, 013602 (2006).

[82] P. Castorina, M. Grasso, M. Oertel, M. Urban, and D. Zappala, Phys. Rev. A **72**, 025601 (2005).

[83] T. Mizushima, K. Machida, and M. Ichioka, Phys. Rev. Lett. **94**, 060404 (2005).

[84] K. Machida, T. Mizushima, and M. Ichioka, Phys. Rev. Lett. **97**, 120407 (2006).

[85] H. Hu, X.-J. Liu, and P. D. Drummond, Phys. Rev. Lett. **98**, 070403 (2007).

[86] M. Gaudin, Phys. Lett. **24A**, 55 (1967).

[87] M. Takahashi, Prog. Theor. Phys. **44**, 348 (1970).

[88] V. Ya. Krivnov and A. A. Ovchinnikov, Zh. Eksp. Teor. Fiz. **67**, 1568 (1974) [Sov. Phys. JETP **40**, 781 (1975)].

[89] M. T. Batchelor *et al.*, J. Phys.: Conf. Ser. **42**, 5 (2006).

[90] X.-W. Guan, M. T. Batchelor, C. Lee, and M. Bortz, Phys. Rev. B **76**, 085120 (2007).

[91] X.-J. Liu, P. D. Drummond, and H. Hu, Phys. Rev. Lett. **94**, 136406 (2005).

[92] G. Orso, Phys. Rev. Lett. **98**, 070402 (2007).

[93] K. Yang, Phys. Rev. B **63**, 140511(R) (2001), and references therein.

[94] K. Machida and H. Nakanishi, Phys. Rev. B **30**, 122 (1984).

[95] A. I. Buzdin and S. V. Polonskii, Zh. Eksp. Teor. Fiz. **93**, 747 (1987) [Sov. Phys. JETP **66**, 422 (1987)].

[96] H. Moritz, T. Stöferle, M. Köhl, and T. Esslinger, Phys. Rev. Lett. **91**, 250402 (2003).

[97] H. Moritz, T. Stöferle, K. Guenter, M. Köhl, and T. Esslinger, Phys. Rev. Lett. **94**, 210401 (2005).

[98] K. V. Kheruntsyan, D. M. Gangardt, P. D. Drummond, and G. V. Shlyapnikov, Phys. Rev. Lett. **91**, 040403 (2003); P. D. Drummond, P. Deuar, and K. V. Kheruntsyan, *ibid.* **92**, 040405 (2004).

[99] K. V. Kheruntsyan and P. D. Drummond, Phys. Rev. A **61**, 063816 (2000); S. J. J. M. F. Kokkelmans, J. N. Milstein, M. L. Chiofalo, R. Walser, and M. J. Holland, *ibid.* **65**, 053617 (2002); P. D. Drummond and K. V. Kheruntsyan, *ibid.* **70**, 033609 (2004).

[100] R. Diener and T.-L. Ho, e-print arXiv:cond-mat/0405174.

[101] X.-J. Liu and H. Hu, Phys. Rev. A **72**, 063613 (2005).

[102] T. Bergeman, M. G. Moore, and M. Olshanii, Phys. Rev. Lett. **91**, 163201 (2003).

[103] G. E. Astrakharchik, D. Blume, S. Giorgini, and L. P. Pitaevskii, Phys. Rev. Lett. **93**, 050402 (2004).

[104] Note the difference in the definition of a_ρ with [102], which accounts for $A = -\zeta(1/2)/\sqrt{2} \simeq 1.0326$.

[105] I. V. Tokatly, Phys. Rev. Lett. **93**, 090405 (2004).

[106] J. N. Fuchs, A. Recati, and W. Zwerger, Phys. Rev. Lett. **93**, 090408 (2004).

[107] E. H. Lieb and W. Liniger, Phys. Rev. **130**, 1605 (1963).

[108] W. Zwerger, J. Opt. B: Quantum Semiclassical Opt. **5**, S9 (2003).

[109] M. Bartenstein *et al.*, Phys. Rev. Lett. **94**, 103201 (2005).

[110] P. de Gennes, *Superconductivity of Metals and Alloys* (Addison-Wesley, New York, 1966).

[111] J. Reidl, A. Csordas, R. Graham, and P. Szepfalusy, Phys. Rev. A **59**, 3816 (1999).